Theory of Giant Magnetoresistance and Tunneling Magnetoresistance

1

Xiaoguang Zhang and William Butler

Contents

X. Zhang (✉)
Department of Physics and Quantum Theory Project, University of Florida, Gainesville, FL, USA

Computer Science and Mathematics Division and Center for Nanophase Materials Sciences, Oak Ridge National Laboratory, Oak Ridge, TN, USA
e-mail: xgz@ufl.edu

W. Butler
MINT Center, University of Alabama, Tuscaloosa, AL, USA
e-mail: wbutler@mint.ua.edu

Y. Xu et al. (eds.), *Handbook of Spintronics*,
DOI 10.1007/978-94-007-6892-5_2

Abstract

This chapter describes the theory of the giant magnetoresistance effect and the tunneling magnetoresistance effect. Giant magnetoresistance and tunneling magnetoresistance arise when a magnetic field reorients the magnetization in different regions of a specimen causing a change in electrical resistance. Typically these regions are different ultrathin layers. Giant magnetoresistance can occur in metallic multilayers. Two geometries are important. Current-in-plane GMR was the first "spintronic" effect and was discovered in 1988. Current-perpendicular-to-plane GMR was observed a few years later and is conceptually easier to understand than current-in-plane GMR. In this chapter both of these phenomena are treated in a semiclassical approximation. For current-in-plane GMR, it is necessary to treat the transport as nonlocal. For current-perpendicular-to-plane GMR, a local approximation is often adequate. Tunneling magnetoresistance arises when quantum mechanical tunneling between ferromagnetic electrodes through an insulating layer depends on the relative orientation of the magnetizations of the two electrodes. In this chapter, tunneling magnetoresistance is treated using the Landauer approach which envisions ballistic electrons traveling between reservoirs with given chemical potentials being transmitted or reflected by the insulating layer. The tunneling current through the layer is carried by the evanescent states. The properties of these evanescent states and how they join to those electronic states near the Fermi energy of the electrodes for the majority and minority spin channels can be important for the size of the tunneling magnetoresistance effect.

List of Abbreviations

AP	Antiparallel
bcc	Body-centered cubic
CIP	Current-in-plane
CPP	Current-perpendicular-to-plane
FERPS	Free electrons with random point scatterers
FM	Ferromagnetic
GMR	Giant magnetoresistance
MR	Magnetoresistance
MTJ	Magnetic tunnel junction
P	Parallel
SAF	Synthetic antiferromagnet
TMR	Tunneling magnetoresistance
XMCD	X-ray magnetic circular dichroism

Introduction

Magnetoresistance refers to a change in the resistance of a material or structure caused by the application of a magnetic field. In this chapter we will discuss two types of magnetoresistance that can occur in structures containing ferromagnetic regions separated by nonmagnetic regions, giant magnetoresistance (GMR) and tunneling magnetoresistance (TMR). One important function of the nonmagnetic regions is to interrupt the short range interatomic exchange interactions that align the magnetic moments of a ferromagnet. This allows the magnetization of the different ferromagnetic regions to have different orientations. Figure 1 is intended to indicate that the ferromagnetic and nonmagnetic regions can have general shapes and distributions. It is more usual for the ferromagnetic and nonmagnetic layers to be alternating layers as described in section "Two-Current Model."

GMR and TMR both occur when a change in the relative orientation of the magnetization in different regions causes a change of the electrical resistance. They differ in the type of material that separates the ferromagnetic regions. For GMR, the separating material is metallic. For TMR the separating material is insulating but very thin so that electrons can travel from one (metallic) magnetic layer to another via quantum mechanical tunneling through the separating layer.

Electron Spin

Magnetism is closely related to the angular momentum of charged particles. For example, the familiar law of Biot-Savart gives the magnetic field caused by a charged particle in motion in terms of its angular momentum relative to the observation point. A collection of such moving charged particles can give rise to a current distribution that generates a magnetic moment. For example, the persistent currents associated with the orbital motion of electrons around a nucleus in an atom generate a magnetic moment that is proportional to the net orbital angular momentum. The proportionality constant, known as the orbital gyromagnetic ratio is $\gamma = e/(2m_e) \approx 0.88 \times 10^{11}\mathrm{C/Kg}$.

However, the translational (or orbital) motion of the electrons is not the only source of angular momentum and magnetic moment in a material. In addition to the orbital angular momentum associated with their motion around the nucleus, electrons have an additional intrinsic angular momentum independent of any translational or orbital motion that we call "spin" angular momentum.

It is difficult to develop an accurate classical picture for electron spin. We could imagine, for example, a classical electron as a spinning top. A spinning charged object will certainly generate a magnetic moment, but the observed gyromagnetic ratio for spin angular momentum is slightly greater than twice the gyromagnetic ratio calculated for the orbital or translational electron motion. Accommodating this observation within a classical picture of an electron as a spinning charge and mass

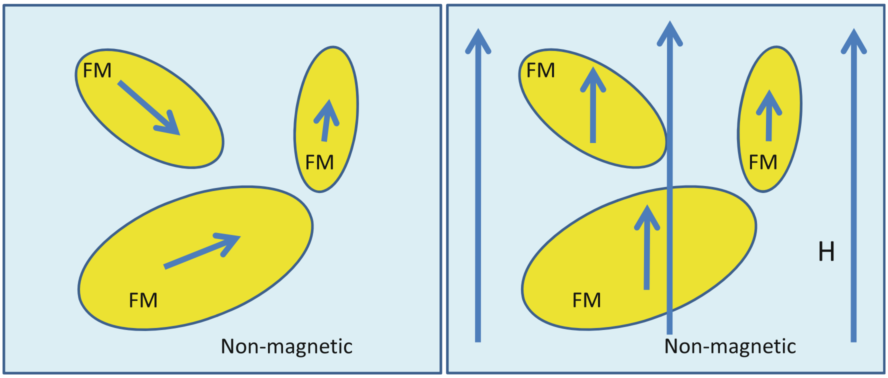

Fig. 1 GMR and TMR arise when a magnetic field reorients the magnetization in different regions causing a change in electrical resistance

distribution would require the charge distribution to be different from the mass distribution. Unfortunately for this classical picture, the electron seems to have no discernable structure at all.

The spin and magnetic moment of the electron arise naturally from the Dirac equation [1]. The intrinsic spin angular momentum of the electron is $\hbar/2$, and its magnetic moment from the Dirac equation is $e\hbar/(2m_e)$. Thus, the gyromagnetic ratio for the electron's spin angular momentum is twice that for its orbital or translational angular momentum (this factor is actually slightly greater (2.002319) due to corrections from quantum electrodynamics). According to the laws of quantum mechanics, the angular momentum vector of a particle with spin $\hbar/2$ can be either aligned or anti-aligned with an arbitrarily chosen quantization axis. We usually choose the quantization axis to be in the z-direction and denote the electrons as up spin or down spin depending on whether they are aligned or anti-aligned with it.

In atoms, the spin and orbital angular momentum are intimately coupled. Closed electron shells in both atoms and solids are simple because both the total orbital and total spin angular momentum for a filled shell vanishes. For the valence electrons of atoms, quantum mechanics tells us how to add the angular momenta of the individual electrons to get the total angular momentum and magnetic moment of a particular atomic state, and there are Hund's rules for determining which of these states has the lowest energy.

In solids, the valence electrons interact with multiple ions and so no longer experience a purely central potential with the consequence that the orbital angular momentum is largely "quenched." Experimental evidence for this "quenching" comes from the measured magnetic moments of transition metal ions in ionic solids and from XMCD (X-ray magnetic circular dichroism) measurements in which the absorption spectra of X-rays with left and circularly polarized light are compared. Analysis of these spectra allows in favorable cases for the determination of both the spin and orbital magnetic moments The detailed XMCD study of spintronic materials is presented in ▶ Chap. 19, “Magnetic Dichroism Studies of Spintronic Structures”, Part VII, by Liu et al. Usually, the spin-magnetic moment is observed to be at least one order of magnitude larger than the orbital magnetic moment.

One important exception to this rule is materials which contain rare earth and actinide atoms. These atoms have unfilled *f*-shells which are very near the nucleus and shielded by the valence electrons from the electric fields produced by neighboring atoms. Such electrons experience a nearly spherical potential and consequently can have large orbital angular momentum. Even for these materials, it is expected that the orbital angular momentum associated with the itinerant current carrying electrons would be small.

Two-Current Model

The preceding paragraphs amount to a very long-winded way of saying that to a very good approximation, one that is better for materials with small atomic numbers, many materials behave as if they are inhabited by two materials, one made up of the up-spin electrons and the other by the down-spin electrons. The approximation of independent up- and down-spin electrons is not as accurate for materials with high atomic numbers because the strong Coulomb field of the nucleus causes the orbital velocity of the electrons to be high leading to a relativistic effect which couples the orbital and spin angular momenta.

Thus, the key to understanding the GMR effect is that the electric current in a GMR device is carried by two different types of electrons. In most materials there are equal numbers of the two types of electrons when they are in equilibrium; however, in ferromagnetic materials there will be more of one type than the other leading to a net magnetic moment. In these materials, electrons having spin moment along the direction of the total (net) magnetic moment of the material are called majority spin (or up spin), while the other types with spin moment opposite the total moment are called minority spin (or down spin).

The number of up-spin and down-spin electrons can change through [2] spin-flip scattering from magnetic impurities that are not collinear with the electron spin, through electron-electron scattering or through spin-orbit coupling. In the 3d-transition metal series, these effects can be relatively weak so that the assumption of two separate conduction channels, one for each spin, with negligible interaction between them, is often a good approximation.

Giant Magnetoresistance

Two basic geometries are used in practical implementations of giant magnetoresistance. Both use alternating layers of ferromagnetic and nonmagnetic materials. For the current-in-plane (CIP) implementation, the electric current flows parallel to the layers, and for the current-perpendicular-to-plane (CPP) implementation, the electric current flows perpendicular to the layers (Fig. 2).

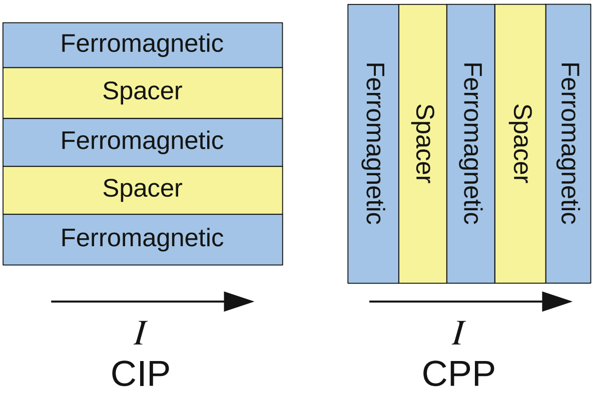

Fig. 2 Different geometries of GMR devices

CIP devices are usually easier to make. This geometry was used in the original experiments by Fert et al. [3] and by Grünberg [4] which led to the 2007 Nobel Prize in Physics. Fert's team deposited a magnetic multilayer in which thin layers of Fe alternated with thin layers of Cr. When they did their experiments in 1987, it had recently been demonstrated that if the Cr layer thicknesses were within certain ranges, the magnetization of alternate Fe layers would be antiparallel [2]. When Fert's team applied a magnetic field that forced the magnetization of all of the Fe layers to align in a common direction, the resistance decreased by a factor of about 2. They described this very large change in resistance as a "giant" magnetoresistance, which became the name of the phenomenon and is applied even when the magnetoresistance is not so large.

The origin of the CIP-GMR effect is somewhat subtle and requires an understanding of transport that goes beyond the local version of Ohm's law. The origin of CPP GMR by contrast can be explained in simple terms, but the phenomenon has its own subtleties. We shall see that a consistent theory of CPP GMR requires that we include the scattering of electrons between the spin channels.

Experimentally, CIP GMR is easier to detect. Typically, the current flows in the plane of a thin multilayered film. The primary challenge is making the layers sufficiently thin compared to the mean free path of the electrons and controlling the relative orientation of the magnetic moments in the ferromagnetic layers.

In contrast, the CPP geometry presents the additional challenge of measuring the resistance of a film perpendicular to the layers. In order for the CPP structure to produce a large enough signal, the resistance of the stack must be measurable in the presence of the resistance of the leads and other parts of the circuit. Various approaches have been used to detect and measure CPP GMR. One way is to reduce the cross section of the layers to the nanometer range. Another way is to stack a large number of layers in the sample, increasing the total thickness of the sample. The difficulty with this approach is that as the number of layers is increased, it may be harder to keep the spacer layer thickness uniform in order to maintain antiferromagnetic coupling across every spacer layer between neighboring ferromagnetic layers. A third approach uses superconducting leads to minimize their resistance relative to the GMR part of the circuit. CPP GMR was successfully measured [5] 3 years after the initial discovery of CIP GMR.

Two-Current Model for a Homogeneous System

When a field is applied to a homogeneous material, the up- and down-spin electrons will both contribute to the total current density, and over a scale much larger than the electron mean free path, we can write Ohm's law as

$$\mathbf{J} = \left(\sigma_\uparrow + \sigma_\downarrow\right)\mathcal{E}. \tag{1}$$

Multiplying by the area and writing the electric field, $\mathcal{E}$, as the potential difference divided by the thickness $\Delta V/t$, we have

$$I = \left(\sigma_\uparrow + \sigma_\downarrow\right)A\Delta V/t \tag{2}$$

which gives the unsurprising result that the resistance is given by the parallel resistor formula

$$R = \frac{\Delta V}{I} = \frac{1}{\left(\sigma_\uparrow + \sigma_\downarrow\right)\frac{A}{t}} = \frac{1}{\frac{1}{R_\uparrow} + \frac{1}{R_\downarrow}} = \frac{R_\uparrow R_\downarrow}{R_\uparrow + R_\downarrow}. \tag{3}$$

In other words, when the spin-flip scattering is neglected, and when we assume a local relationship between current and field as implied by Eq. 1, the two spin channels behave like two parallel conduction channels, each with its own resistance $R_\uparrow$ and $R_\downarrow$. For the CPP geometry, this provides the basis for a very simple mechanism of GMR.

Parallel-Resistors-in-Series Model for CPP GMR

One type of CPP-GMR system consists of a stack of ferromagnetic/nonmagnetic metallic layers. The nonmagnetic spacer layer has a carefully controlled thickness that gives the antiferromagnetic coupling between the two ferromagnetic layers that it separates. The structure may be repeated for as many periods as the fabrication technique allows without losing the antiferromagnetic coupling across the spacer layers.

As shown in Fig. 3, the resistors-in-series model for such a system is simply a network of two parallel series of resistors, each series representing a spin channel. If the nonmagnetic spacer layers are chosen correctly and have the correct thickness, the magnetic configuration for zero applied magnetic field is an alternating up-down alignment of the ferromagnetic layers. Assuming that all ferromagnetic layers have the same thickness and that there is an even number of

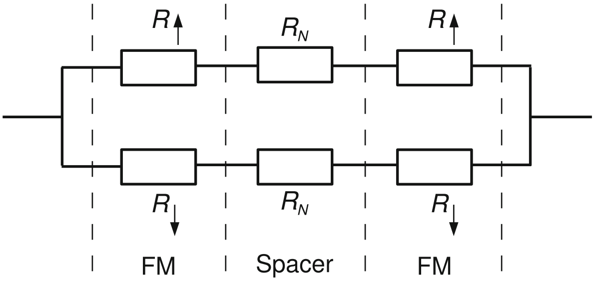

Fig. 3 Two-current circuit model for a magnetic multilayer in the CPP geometry. The parallel or aligned moment magnetic configuration is shown

ferromagnetic layers, the resistances for the two spin channels are the same and are given by

$$R_{\uparrow}^{AP} = R_{\downarrow}^{AP} = \frac{n}{2}\left(R_{\uparrow}^{F} + R_{\downarrow}^{F}\right) + 2nR_N, \tag{4}$$

where the superscript AP stands for antiparallel. $R_{\uparrow(\downarrow)}^{F}$ are the ↑ (↓) spin channel resistance for a single ferromagnetic layer, R_N is the total resistance for a single spacer layer ($2R_N$ is the resistance for each spin channel), and n is the number of bilayers including one ferromagnetic layer and a nonmagnetic spacer layer. The total resistance of the stack is

$$R^{AP} = \frac{R_{\uparrow}^{AP} R_{\downarrow}^{AP}}{R_{\uparrow}^{AP} + R_{\downarrow}^{AP}} = \frac{n}{4}\left(R_{\uparrow}^{F} + R_{\downarrow}^{F} + 4R_N\right). \tag{5}$$

When a magnetic field is applied to align the moments in all of the ferromagnetic layers, the resistance for each spin channel is different. Now we have

$$R_{\uparrow(\downarrow)}^{P} = n\left[R_{\uparrow(\downarrow)}^{F} + 2R_N\right], \tag{6}$$

where the superscript P stands for parallel, indicating that the moments in all of the ferromagnetic layers are now parallel to each other. The total resistance for P is

$$R^{P} = \frac{R_{\uparrow}^{P} R_{\downarrow}^{P}}{R_{\uparrow}^{P} + R_{\downarrow}^{P}} = n\frac{\left[R_{\uparrow}^{F} + 2R_N\right]\,\left[R_{\downarrow}^{N} + 2R_N\right]}{R_{\uparrow}^{F} + R_{\downarrow}^{F} + 4R_N}. \tag{7}$$

From Eqs. 5 and 7, we can obtain a simple relationship

$$\sqrt{\left(R^{AP} - R^{P}\right)\ R^{AP}} = \frac{n}{4}\left|R_{\uparrow}^{F} - R_{\downarrow}^{F}\right|. \tag{8}$$

It is often convenient to separate the effect of interface spin-dependent scattering from the bulk resistance. To do this we replace the resistance, R_s, for each spin channel in the ferromagnetic layer by the sum $R_s + 2r_s$ where r_s is the resistance at a single interface. Then the above equation becomes

$$\sqrt{\left(R^{AP} - R^{P}\right)\ R^{AP}} = \frac{n}{4}\left|R^F_\uparrow - R^F_\downarrow\right| + \frac{n}{2}\left|r_\uparrow - r_\downarrow\right|. \tag{9}$$

Multiplying by A on both sides, we finally obtain

$$\sqrt{\left(R^{AP} - R^{P}\right)R^{AP}}A = \left|\rho_\uparrow - \rho_\downarrow\right|\frac{t_F}{(t_F + t_N)}L + \frac{nA}{2}\left|r_\uparrow - r_\downarrow\right|, \tag{10}$$

where t_F and t_N are the thicknesses of single ferromagnetic and nonmagnetic layers, respectively, $R^F_{\uparrow(\downarrow)} = \rho_{\downarrow(\uparrow)}t_F/A$, and L is the total thickness of the sample.

If the resistance of the spacer layers, R_N, is negligible, we obtain a simple expression for the CPP magnetoresistance

$$MR = \frac{R^{AP}}{R^P} - 1 = \frac{\left(R^F_\uparrow - R^F_\downarrow\right)^2}{4R^F_\uparrow R^F_\downarrow} = \frac{\left(\rho_\uparrow - \rho_\downarrow\right)^2}{4\rho_\uparrow\rho_\downarrow} = \frac{1}{4}\left(\frac{\rho_\uparrow}{\rho_\downarrow} + \frac{\rho_\downarrow}{\rho_\uparrow} - 2\right). \tag{11}$$

Thus, in an ideal CPP-GMR sample, the magnetoresistance in this model is simply a function of the resistivity ratio between the two spin channels of the ferromagnetic layers. The larger the ratio of the resistivities of the two spin channels, the larger the GMR.

One important result of the resistors-in-series model for CPP is the prediction that the electrochemical potential for the two spin channels at the same point in space can be different. This difference is largest in the AP configuration. To see this, let us examine a trilayer whose spacer layer resistance R_N is negligible. For the AP configuration, the currents in the two spin channels are the same and each is given by

$$I_\uparrow = I_\downarrow = \frac{V}{R^F_\uparrow + R^F_\downarrow}, \tag{12}$$

where V is the total voltage across the trilayer. The electrochemical potential in the spacer layer for the up (down)-spin electrons is

$$V_{\uparrow(\downarrow)} = V - I_{\uparrow(\downarrow)}R^F_{\uparrow(\downarrow)} = \frac{VR^F_{\uparrow(\downarrow)}}{R^F_\uparrow + R^F_\downarrow}. \tag{13}$$

The potential difference between the two spin channels in the low-resistance spacer layer which separates them is

$$V_\uparrow - V_\downarrow = V\frac{R_\downarrow^F - R_\uparrow^F}{R_\uparrow^F + R_\downarrow^F}. \tag{14}$$

Another curiosity of the parallel-resistors-in-series model can be seen in the parallel moment configuration. Let us suppose that the leads in Fig. 3 are nonmagnetic. In this case we expect equal currents to be transported by the two spin channels in the leads. However, that is clearly not the case for this model. We will see in section "Spin-Flip Scattering and the Drift-Diffusion Model" how the model can be extended to provide a more physical picture.

Although the parallel-resistors-in-series model for GMR gives us a quick and simple picture that helps us understand the origin of GMR, it needs improvement in two distinct ways. We will need to include spin-flip scattering to obtain a realistic treatment of CPP GMR, and we will need to include the effects of a finite electron mean free path to obtain any CIP GMR at all.

Spin-Dependent Resistivity of Ferromagnetic Metals

The discussion above makes it clear that one key to obtaining a GMR is choosing materials with a large difference in the resistivities of the two spin channels in the ferromagnetic layer. Because of differences in the electronic structure between the two spin channels in ferromagnetic metals, their resistivities may be quite different even if the scattering lifetimes are similar between the two channels. For clean films at room temperature, the scattering is dominated by phonon scattering, whose scattering rate is roughly proportional to the electron density of states at the Fermi energy, which in turn is inversely proportional to the Fermi velocity for a single band. Therefore, there is also a tendency for the scattering lifetime to be approximately proportional to the Fermi velocity. Furthermore, because the electron mean free path l is the product of the Fermi velocity v_F and the scattering lifetime τ,

$$l = v_F\tau; \tag{15}$$

the fact that v_F and τ tend to trend together magnifies the difference in the mean free path between the two spin channels. This is indeed the case in Table 1, where we list the typical values of the average Fermi velocity v_F calculated from band structures, the estimated mean free path l from experimental measurements, the electron-scattering lifetime $\tau = l/v_F$, and the resistivity ρ per spin channel estimated from an integration over the Fermi surface using the other parameters as input, for ferromagnetic metals Fe and Co, as well as for nonmagnetic Cu. In this table we see that there are significant differences between the majority and minority spin mean free paths for both Fe and Co films. In the case of Co, this translates into a very large difference in the resistivities of the two spin channels. Using Eq. 11 and the values in Table 1, we estimate that the maximum CPP GMR that can be achieved in an ideal Co/Cu multilayer is about

Table 1 Typical values of average Fermi velocity v_F, mean free path l, scattering lifetime τ, and resistivity ρ per spin channel in sputtered films of ferromagnetic metals. Also listed are the values for nonmagnetic copper films. Mean free path data is from Ref. [39]

Metal	v_F (10^7 cm/s)	l (Å)	τ (10^{-15} s)	$\rho_{\uparrow(\downarrow)}$ (μΩ cm)
Fe majority	3.3	15	4.5	49
Fe minority	4.1	21	5.1	65
Co majority	7.9	55	7.0	32
Co minority	2.7	6	2.2	141
Cu	10.7	300	28	4.6

$$MR \approx \frac{\left(\rho_\uparrow - \rho_\downarrow\right)^2}{4\rho_\uparrow\rho_\downarrow} \approx 66\%. \tag{16}$$

Actual Co/Cu multilayers are far from ideal, and the measured MRs are significantly less than this value.

The case of Fe is a little more complicated. The minority spin channel in Fe has a longer mean free path. But this does not translate into a smaller resistivity. Instead, the Fe majority spin has a smaller resistivity. This is because another factor plays the opposite role and overwhelms the difference in the mean free path. Fe majority spin has more bands than the minority spin. This translates into more conduction channels and results into a smaller resistivity. However, the difference in the resistivity as listed in Table 1 is not enough to give the amount of MR measured in Fe/Cr multilayers. Using Eq. 11 and the values for Fe in Table 1, we find an MR of only 2 %, far less than the 10 % observed in experiments. What are we missing?

The missing ingredient is the intermixing of Fe and Cr atoms. When Cr atoms get into the Fe layer, they become strongly spin-dependent scattering centers. To see qualitatively how Cr impurities scatter differently in the two spin channels, we can simply count the number of valence electrons in each spin channel for Fe and Cr. Because both Fe and Cr bulk metals have the bcc structure, they have nearly the same band structure, with the difference in the position of the Fermi energy relative to the majority and minority spin bands. We write the total number of valence electrons per atom as

$$N = N_\uparrow + N_\downarrow, \tag{17}$$

where the arrows indicate the number of electrons in the majority (↑) and the minority (↓) spin channels, and the total magnetic moment as

$$M = \left(N_\uparrow - N_\downarrow\right)\mu_B. \tag{18}$$

The number of valence electrons for Cr is 6 and for Fe is 8, and the moments are 0 for Cr (neglecting its weak antiferromagnetism) and 2 μ_B for Fe, respectively. From these values we find that both Cr and Fe have the same number of minority spin electrons ($N_\downarrow = 3$), but very different numbers of majority spin electrons ($N_\uparrow = 3$ for Cr and 5 for Fe). Thus, for the down-spin electrons, the Cr atom looks very similar to the Fe atom. This yields minimal scattering for electrons and a low resistance. On the other hand, the majority spin potential for the Cr atom is very different than that of the Fe atom; thus, a Cr impurity in Fe can cause strong scattering in the majority spin channel, leading to a large resistance for the majority spin.

Not all intermixing will increase GMR. In the case of Fe/Cu or permalloy/Cu multilayers (permalloy is $Ni_{80}Fe_{20}$ alloy), significant intermixing near the interfaces will produce magnetic impurities with loose spins, whose magnetic moment is not aligned, neither parallel nor antiparallel to the moment of the ferromagnetic layer, or even magnetic dead layers. Loose spins increase spin-flip scattering, and dead layers introduce significant parasitic resistance. Both can reduce the GMR.

There is an interesting connection between GMR and the Slater-Pauling rule. The Slater-Pauling rule [6, 7] pertains to 3*d*-transition metal alloys but has been generalized to other alloy systems. It notes a tendency of bcc and related alloys of 3d-transition metals to prefer to have 3 electrons per atom in the minority spin channel. This can lead to weak scattering in this channel as all of the 3d species adjust their magnetic moments so that their d-bands are nearly degenerate. The Slater-Pauling rule also notes a tendency for fcc-based alloys of 3d-transition metals to adjust their magnetic moments so that the majority d-band is filled. This can lead to weak scattering in the majority channel for these alloys because all atoms will have approximately 5.3 electrons in the majority channel.

Limitation of the Parallel-Resistors-in-Series Model

Although the parallel-resistors-in-series model can successfully explain the existence of CPP GMR, neglecting the spin-flip scattering can sometimes lead to very wrong predictions. Here we give an example of a widely used multilayer system for which this model fails.

We have explained that in order to obtain a large CPP GMR in multilayer systems, we want the zero field state be such that the moments in neighboring magnetic layers are antiparallel to each other, in what we call an *AP* configuration. This way when a small magnetic field is applied, it aligns the moment in all the ferromagnetic layers into the same direction, in what we call a *P* configuration, reducing the total resistance and resulting in the GMR effect. In a practical setup, it is often difficult to keep the spacer layer thickness at exactly the optimal point to ensure the antiferromagnetic coupling. Variations in the spacer layer thickness can greatly diminish or even eliminate the GMR effect.

Many recent designs adopted an approach that uses a synthetic antiferromagnet (SAF) [8]. The basic idea is to have one of the ferromagnetic layers (free layer) rotate freely with the applied magnetic field and to have other ferromagnetic layers stay fixed (reference layer). To remove the effect of the magnetic field on the reference layer, two strongly antiferromagnetically coupled magnetic layers are used. Because they always align opposite each other, the total magnetic moment adds to zero. Thus, these two layers will not be rotated by the magnetic field.

The free layer is usually a soft magnetic material such as the permalloy. The SAF layer is a sandwich consisting of CoFe/Ru/CoFe. A typical stack of Py/Cu/CoFe/Ru/CoFe (where Py stands for permalloy) would have the desired magnetic configurations tunable by the applied magnetic field and would often show a few percent magnetoresistance.

Let us now apply the parallel-resistors-in-series model to this system. For the sake of simplicity, let us assume that the two CoFe layers in the SAF have the same thickness and thus the same resistance. Let us also neglect the resistance of Ru and Cu layers. The parallel (P) configuration is when the permalloy moment aligns with the neighboring CoFe layer, and the AP configuration is when their moments are oppositely aligned. The resistance for each spin channel in the P configuration is

$$R^{P}_{\uparrow(\downarrow)} = R^{\mathrm{Py}}_{\uparrow(\downarrow)} + R^{\mathrm{CoFe}}_{\uparrow(\downarrow)} + R^{\mathrm{CoFe}}_{\downarrow(\uparrow)}. \tag{19}$$

For the AP configuration, the resistance is

$$R^{AP}_{\uparrow(\downarrow)} = R^{\mathrm{Py}}_{\downarrow(\uparrow)} + R^{\mathrm{CoFe}}_{\uparrow(\downarrow)} + R^{\mathrm{CoFe}}_{\downarrow(\uparrow)}. \tag{20}$$

It is clear that $R^{AP}_{\downarrow} = R^{P}_{\uparrow}$ and $R^{AP}_{\uparrow} = R^{P}_{\downarrow}$. Consequently, the total resistance $R^{P} = R^{AP}$ and the parallel-resistors-in-series model predicts zero magnetoresistance for the system with the SAF reference layer which is known experimentally to work very well!

The problem is in the neglected spin-flip scattering. The Ru layer in the SAF stack has a strong spin-orbit coupling. This causes a significant spin-flip term in the Ru layer. The circuit model of two independent parallel paths is no longer valid. Instead, there is a cross path mixing the two spin channels. Let us consider the extreme case that the two spin channels are completely mixed inside the Ru layer, i.e., $\tau^{\mathrm{Ru}}_{\uparrow\downarrow} = 0$. In this limit, the last CoFe layer does not play any role in the magnetoresistance except for adding to an additional parasitic resistance term. The stack Py/Cu/CoFe is similar to a trilayer spin-valve structure. Applying the parallel-resistors-in-series model only to the trilayer, the magnetoresistance is

$$\mathrm{MR} = \frac{\left(R^{\mathrm{Py}}_{\uparrow} - R^{\mathrm{Py}}_{\downarrow}\right)\left(R^{\mathrm{CoFe}}_{\uparrow} - R^{\mathrm{CoFe}}_{\downarrow}\right)}{\left(R^{\mathrm{Py}}_{\uparrow} + R^{\mathrm{CoFe}}_{\uparrow}\right)\left(R^{\mathrm{Py}}_{\downarrow} + R^{\mathrm{CoFe}}_{\downarrow}\right)}. \tag{21}$$

This example demonstrates that a complete theoretical description of the GMR must include the effect of spin-flip scattering.

Spin-Flip Scattering and the Drift-Diffusion Model

As pointed out in section "Limitation of the Parallel-Resistors-in-Series Model," a useful theory of CPP GMR must include processes that return the spin densities to their equilibrium distributions in the presence of spin-flip scattering. A simple model that does this was developed by Valet and Fert [9] who extended earlier work by Johnson and Silsbee [10]. The Valet-Fert equations can be derived as an approximation to the Boltzmann transport equation for an extended homogeneous system. Application to layered systems requires additional approximations.

In this section we will obtain the Valet-Fert equations by a more heuristic route. We saw in section "Parallel-Resistors-in-Series Model for CPP GMR" that the up- and down-spin electrons can experience a different electrical potential in CPP geometry. This comes about because different conductivities for the up-spin and down-spin electrons lead to different Ohm's law voltage drops. At the same time, it is clear that the voltage-induced spin-dependent currents must affect the density of the spins if we are to have equal spin currents in the leads and unequal spin currents through the effective resistors of Fig. 3. The first Valet-Fert equation is Ohm's law applied to the individual spin channel microscopically, in the form

$$\mathbf{J}_s = \frac{\sigma_s}{e} \nabla \overline{\mu}_s, \tag{22}$$

where $\mathbf{J}_s$ is the current density for spin s, σ_s is the spin-dependent conductivity, and $\overline{\mu}_s = \mu_s - eV$ is the local electrochemical potential for spin s. Thus, the spin-dependent current in this generalization of Ohm's law flows not only in response to the microscopic electric field $-\nabla V$ but also in response to a local accumulation of spin density described by a spatially varying spin-dependent chemical potential, $\nabla \mu_s$.

Since electrons are neither created nor destroyed in an electrical circuit, in steady state, the divergence of the total current vanishes, $\nabla \cdot \mathbf{J} = 0$. However, if there is spin-flip scattering, up spins can be converted into down spins and vice versa. The continuity theorem tells us that

$$\nabla \cdot \mathbf{J}_s = -e \frac{\partial n_s}{\partial t}, \tag{23}$$

where n_s is the density of spins of type s. The density of electrons with spin s will be given in terms of the Fermi function as

$$n_s = \frac{1}{V} \sum_k f_0(E_{ks} - \mu_s), \tag{24}$$

and its rate of change will be given in terms of the Fermi energy density of states, N_s as

$$\frac{\partial n_s}{\partial t} = -\sum_k \frac{\partial f_0(E_{ks} - \mu_s)}{\partial E_{ks}} \frac{\partial \mu_s}{\partial t} = N_s \frac{\partial \mu_s}{\partial t}. \tag{25}$$

The rate of change of the chemical potentials depends on how far out of balance they are (i.e., the magnitude of $\mu_s - \mu_{-s}$), and on the rate of spin-flip scattering $1/\tau^{sf}$,

$$\frac{\partial \mu_s}{\partial t} = -\frac{(\mu_s - \mu_{-s})}{\tau^{sf}}. \tag{26}$$

One of the great advantages of Valet-Fert theory is its parsimonious usage of material parameters. For a system with cubic symmetry, the Fermi energy density of states, N_s, is related to the conductivity through

$$\sigma_s = \frac{e^2}{3}\left\langle v_{Fs}^2 \tau_s \right\rangle N_s, \tag{27}$$

where the semiclassical expression for the conductivity due to spin channels of an isotropic or cubic system is

$$\sigma_s = \frac{e^2}{3V}\sum_{\mathbf{k}} -\frac{\partial f_0(E_{s\mathbf{k}} - \mu)}{\partial E_{s\mathbf{k}}} v_{s\mathbf{k}}^2 \tau_{s\mathbf{k}}, \tag{28}$$

and the Fermi energy density of states is given by

$$N_s = \frac{1}{V}\sum_{\mathbf{k}} -\frac{\partial f_0(E_{s\mathbf{k}} - \mu)}{\partial E_{s\mathbf{k}}}. \tag{29}$$

Combining Eqs. 23, 24, 25, 26, and 27, we have

$$\nabla \cdot \mathbf{J}_s = eN_s \frac{(\mu_s - \mu_{-s})}{\tau^{sf}} = \frac{\sigma_s}{e} \frac{(\overline{\mu}_s - \overline{\mu}_{-s})}{\left(l_s^{sf}\right)^2} \tag{30}$$

where we have defined the spin-diffusion length for spin s, l_s^{sf}, through $\left(l_s^{fs}\right)^2 = \left\langle v_{Fs}^2 \tau_s \right\rangle \tau_{sf}/3$.

Insight into the meaning of the spin-diffusion length can be obtained through a random walk argument. Assume that the mean time between scattering events that change the electron's momentum, but not its spin, is τ_s. In reality, this will depend on **k** but we will ignore that for the present argument. If the magnitude of the Fermi velocity is v_{Fs}, the mean distance that the electron travels between these momentum scattering events is $l_s = v_{Fs}\tau_s$. We further assume, after each scattering event, the electron goes off in a random direction completely independent of its direction before the scattering event. This is seldom exactly true, but the error can be at least partially compensated by adjusting the value of the momentum lifetime. We now assume that there will occasionally be a scattering event that also flips the electron's spin. We can view this as a three-dimensional random walk problem in which we ask how far a random walker will get on the average taking $n = \tau^{sf}/\tau_s$ steps of length l_s. The answer (root mean square of distance) is $\sqrt{n/3}l_s$ which is equivalent to the spin-diffusion length defined above.

Using Eq. 22, the continuity equation (charge density does not change in steady state) becomes

$$\nabla^2\left(\sigma_\uparrow\overline{\mu}_\uparrow + \sigma_\downarrow\overline{\mu}_\downarrow\right) = 0. \tag{31}$$

Combining Eqs. 22 and 30, we can obtain

$$\nabla^2\left(\overline{\mu}_\uparrow - \overline{\mu}_\downarrow\right) = \left(\overline{\mu}_\uparrow - \overline{\mu}_\downarrow\right)\left(\frac{1}{l_{sf\uparrow}^2} + \frac{1}{l_{sf\downarrow}^2}\right). \tag{32}$$

The Valet-Fert approximation consists of solving these last two equations for the electrochemical potentials subject to boundary conditions of continuity at the interfaces. We will derive the Valet-Fert equations more properly after we introduce the Boltzmann transport equation.

For simplicity, let us consider a layered system with interfaces perpendicular to the z-direction and assume that Eqs. 31 and 32 which were derived for a homogeneous system can be applied to this layered geometry. Equation 32 becomes

$$\frac{\partial^2 \Delta\mu}{\partial z^2} = \frac{\Delta\mu}{l_{sf}^2} \tag{33}$$

where $\Delta\mu = \left(\overline{\mu}_\uparrow - \overline{\mu}_\downarrow\right)$ and $1/l_{sf}^2 = 1/l_{sf\uparrow}^2 + 1/l_{sf\downarrow}^2$. The general solution to this second-order differential equation is

$$\Delta\mu = A\exp\left(z/l_{sf}\right) + B\exp\left(-z/l_{sf}\right). \tag{34}$$

The corresponding solution to Eq. 31 is

$$\sigma_\uparrow\mu_\uparrow + \sigma_\downarrow\mu_\downarrow = Jz + D, \tag{35}$$

where $J = J_\uparrow + J_\downarrow$ is the total current density. Solving the simultaneous Eqs. 34 and 35 will yield the values for $\mu_\uparrow$ and $\mu_\downarrow$ as functions of z.

For multilayers, one simply stitches the general solutions within each layer together using boundary conditions which are the continuity of the current density and the local electron chemical potential for each spin.

The FERPS Model

The understanding of current-in-plane or CIP GMR requires the combination of two effects. First is the nonlocal conductivity in an inhomogeneous solid. Second is the spin-dependent scattering of electrons. A relatively simple model that can incorporate both effects and generate CIP GMR is the model of free electrons with random point scatterers (FERPS) [11]. This model has been implicitly or explicitly assumed for almost all theoretical works on the GMR that were not based on first-principles electronic structure calculations. In this model one assumes that the scatterers are points, that they are distributed randomly in space, and that there are many scatterers within a region of space of volume ℓ^3 where ℓ is the electron mean free path. Because point scatterers scatter isotropically and do not have the so-called vertex corrections, the first assumption directly allows the use of a relaxation time approximation, which neglects the "scattering-in" term of the Boltzmann equation (sometimes known as the vertex corrections in quantum approaches). Even for many real materials with nearly free-electron-like dispersion, the relaxation time approximation for the impurity scattering is inaccurate. However, when the Fermi energy falls in the d-bands so that the scattering is primarily between s and d states or between two d states, the symmetries of the s and d wave functions are such that the leading order in the vertex corrections tends to vanish. For such materials, the relaxation time approximation may be reasonable.

The assumption of random point scatterers offers an additional simplification. It keeps the effect of scattering local which makes it easier to speak in terms of a local scattering rate or a local mean free path. The FERPS model is certainly a major oversimplification, but it has tradition on its side, and it is sufficiently simple that one may hope to see general features without getting lost in detail. It is also useful for testing first-principles calculations which should be capable of giving the FERPS results in the appropriate limit.

Nonlocal Conductivity

In the macroscopic model for electric conductivity in a metal, the conductivity is always considered to be local. In other words, the electric field at position $\mathbf{r}$ would cause a current density only at the same position, through the local version of the Ohm's law,

$$\mathbf{J}(\mathbf{r}) = \sigma(\mathbf{r})\mathcal{E}(\mathbf{r}). \tag{36}$$

Although the two-current model using local conductivity is adequate to explain CPP GMR (meaning that it gives plausible results), it is not adequate to explain the phenomenon of CIP GMR. It is easy to show that the CIP GMR is exactly zero if the conductivity is completely local.

In a magnetic multilayer, when the current flows within the plane of the layers, the total current is the sum of the current in each layer. If the conductivity is entirely local, then it is easy to show within the two-current model that no GMR will emerge even if there is spin-dependent conductance. For example, consider a ferromagnetic/spacer/ferromagnetic trilayer. If the conductivity is entirely local, then the current within each layer does not depend on the moment orientation of other layers. When the moments of the two ferromagnetic layers are aligned parallel, each spin channel has the total current

$$I_s = I_{1s} + \frac{1}{2} I_2 + I_{3s}, \tag{37}$$

where $s = \uparrow (\downarrow)$ indicates the spin channel and 1, 2, 3 indicates the layer. The total current is the sum over both spin channels,

$$I = I_{1\uparrow} + I_{1\downarrow} + I_2 + I_{3\uparrow} + I_{3\downarrow}. \tag{38}$$

When the moments are aligned antiparallel, the current in one of the spin channels is

$$I_{AP\uparrow} = I_{1\uparrow} + \frac{1}{2} I_2 + I_{3\downarrow}, \tag{39}$$

and in the other spin channels is

$$I_{AP\downarrow} = I_{1\downarrow} + \frac{1}{2} I_2 + I_{3\uparrow}. \tag{40}$$

The sum of Eqs. 39 and 40 is identical to the total current for parallel alignment, Eq. 38. Thus, there would be no magnetoresistance if the conductivity is entirely local.

The picture of a nonlocal conductivity can be understood if we imagine that an electron is accelerated by an electric field at point $\mathbf{r}'$ and flies through the solid for a time τ (the relaxation time of the electrons) before being scattered by an impurity at point $\mathbf{r}$ and dissipating its extra momentum. Chambers [12] presented a semiclassical argument that the energy of an electron passing through point $\mathbf{r}$ at time t had its energy modified by ΔE,

$$\Delta E(\mathbf{r}, t) = \int_{-\infty}^{t} \mathbf{v}'(t') \cdot eE(\mathbf{r}') e^{-(t-t')/\tau} dt', \tag{41}$$

where $\mathbf{v}'$ is the electron velocity at point $\mathbf{r}'$ and time t'. Every electron will have a similar equation due to the applied electric field. Assuming that the electrons were initially in equilibrium before their energy was modified by the applied field, then the distribution of all electrons can be described by a distribution function in the form

$$f(\mathbf{r}, \mathbf{v}, t) = f_0(E) + \frac{\partial f_0}{\partial E} \Delta E(\mathbf{r}, t), \tag{42}$$

where $f_0(E)$ is the equilibrium distribution function which depends only on the electron energy.

The current density is calculated from the average velocity of all electrons,

$$\mathbf{J}(\mathbf{r}) = -\frac{e}{V} \sum_{\mathbf{v}} \mathbf{v} f(\mathbf{r}, \mathbf{v}, t) = -\frac{e}{V} \sum_{\mathbf{v}} \mathbf{v} \frac{\partial f_0}{\partial E} \Delta E(\mathbf{r}, t), \tag{43}$$

where V is the volume of the sample and we used $\sum_{\mathbf{v}} \mathbf{v} f_0(E) = 0$. Substituting Eq. 41 into this, we find

$$\mathbf{J}(\mathbf{r}) = -\frac{e^2}{V}\sum_{\mathbf{v}} \mathbf{v}\frac{\partial f_0}{\partial E}\int_{-\infty}^{t} \mathbf{v}'(t') \cdot \varepsilon[\mathbf{r}'(t')]e^{-(t-t')/\tau}dt'. \tag{44}$$

The current density at position $\mathbf{r}$ depends on the electric field at position $\mathbf{r}'$ parametrically through the time variable t'. For free electrons in a homogeneous medium, the factor $\partial f_0/\partial E$ is essentially a δ function at the Fermi energy, and $\mathbf{v}/v_F = (\mathbf{r} - \mathbf{r}')/|\mathbf{r} - \mathbf{r}'|$. The above expression can be reduced to

$$\mathbf{J}(\mathbf{r}) = \frac{e^2 k_F^2}{(2\pi)^3\hbar}\int d^3\mathbf{R}\frac{\mathbf{R}\mathbf{R}}{R^2} \cdot \varepsilon(\mathbf{r}')e^{-R/\ell}, \tag{45}$$

where $\mathbf{R} = \mathbf{r} - \mathbf{r}'$ and $\ell = \mathbf{v}_F\tau$ is the electron mean free path. In general, if the scattering rate is not homogeneous, then the exponential factor $e^{-(t-t')/\tau}$ in Eq. 44 can be modified as $e^{-\int_{t'}^{t} dt''/\tau(t'')}$. The current density can be written in the form

$$\mathbf{J}(\mathbf{r}) = \int d^3\mathbf{r}'\boldsymbol{\sigma}(\mathbf{r}, \mathbf{r}') \cdot \varepsilon(\mathbf{r}'), \tag{46}$$

where $\sigma(\mathbf{r}, \mathbf{r}')$ is the nonlocal conductivity tensor.

For layered structures, within the FERPS model, we can assume that the material is uniform in the xy directions and drop the dependence on xy. The integration over t' can be converted to integration over z by $dt' = dz'/|\mathbf{v}|\cos\theta$ where θ is the angle between the velocity $\mathbf{v}$ and the z-axis. We further have $t - t' = \int_{z'}^{z} dz''/|\mathbf{v}|\cos\theta$. Thus,

$$\sigma(z, z') = \frac{e^2 m}{2\hbar^3}\int_{-\pi/2}^{\pi/2} \tan\theta d\theta \mathbf{v}_F\mathbf{v}_F e^{-\int_{z'}^{z} dz''/\ell(z'')\cos\theta}, \tag{47}$$

where $\ell(z'') = |\mathbf{v}_F|\tau(z'')$.

We assume that the material properties are uniform within each layer. Thus, the local electric field will have a layer index I instead of coordinate dependence $\mathbf{r}$ and is written as $\mathcal{E}_I$. Similarly the scattering mean free path is ℓ_I, and the layer conductivity is σ_{IJ}. The Camblong-Levy approximation [13] to the conductivity of the multilayer can be obtained by integrating Eq. 47 over z' and averaging over z within the respective layers,

$$\sigma_{xx}^{II} = \sigma_I\left\{1 + \frac{3}{4}\frac{\ell_I}{d_I}\left[-\frac{1}{2} + 2E_3\left(\frac{d_I}{\ell_I}\right) - 2E_5\left(\frac{d_I}{\ell_I}\right)\right]\right\}, \tag{48}$$

and for $I \neq J$,

$$\sigma_{xx}^{IJ} = \frac{3\sigma_I}{4}\frac{\ell_J}{d_I} \quad \begin{aligned} &\left[E_3(\phi_{IJ}) - E_3\left(\phi_{I-1,J}\right) - E_3\left(\phi_{I,J+1}\right) + E_3\left(\phi_{I-1,J+1}\right)\right. \\ &\left.-E_5(\phi_{IJ}) + E_5\left(\phi_{I-1,J}\right) + E_5\left(\phi_{I,J+1}\right) - E_5\left(\phi_{I-1,J+1}\right)\right], \end{aligned} \tag{49}$$

where $\sigma_I = e^2 k_F^2 \ell_I / 6\pi^2 \hbar = n_I e^2 \tau_I / m$, and the ϕ_{IJ} are defined by

$$\phi_{IJ} = \int_{z_{I+1}}^{z_J} \frac{dz}{\ell(z)} \quad (I < J), \tag{50}$$

where $d_I = z_{I+1} - z_I$, and the functions $E_n(x)$ are the exponential integrals defined by

$$E_n(x) = \int_1^{\infty} \frac{e^{-xt}}{t^n} dt. \tag{51}$$

The total conductance will be given by the sum of these nonlocal conductivities, for example, a trilayer CIP-GMR film with total thickness, d; width, W; and length along field direction, L, would have a different conductance for parallel alignment,

$$G_P = \frac{Wd}{L} \sum_{I,J=1,2,3} \left[\sigma_{xx}^{IJ}\left(\ell_1^{\uparrow}, \ell_2, \ell_3^{\uparrow}\right) + \sigma_{xx}^{IJ}\left(\ell_1^{\downarrow}, \ell_2, \ell_3^{\downarrow}\right)\right], \tag{52}$$

and antiparallel alignment,

$$G_A = \frac{Wd}{L} \sum_{I,J=1,2,3} \left[\sigma_{xx}^{IJ}\left(\ell_1^{\uparrow}, \ell_2, \ell_3^{\downarrow}\right) + \sigma_{xx}^{IJ}\left(\ell_1^{\uparrow}, \ell_2, \ell_3^{\downarrow}\right)\right]. \tag{53}$$

The above Camblong-Levy expressions [13], Eqs. 48 and 49, for the conductivity can also be derived from the Fuchs-Sondheimer theory [14, 15] using a z-dependent lifetime $\tau(z)$ or in the multilayer case τ_I for layer I. Many other authors have also come up with their own derivations of the semiclassical theory using assumptions similar to the FERPS model. All these derivations are completely equivalent. The truncation of the sum over σ^{IJ} in the case of a film with finite thickness is equivalent to complete diffuse surface scattering which would be modeled in Fuchs-Sondheimer theory by $p = 0$ in the boundary conditions at the surfaces.

The conductivity calculated from the semiclassical theory agrees surprisingly well [11] with the numerical evaluation of the Kubo formula, which is the formula that yields the conductivity from a full quantum mechanical approach. Such agreement justifies the use of the semiclassical Boltzmann transport equation for modeling the GMR materials.

When the conductivity is nonlocal, the current within each layer has a contribution due to the field in other layers. Such contribution depends on the moment orientation of both (or all if the term spans across many layers) layers and changes when the moment configuration is changed. This term is the source of CIP GMR. In the classical picture, the contribution consists of terms involving, for example, an electron with a finite transverse momentum being accelerated in layer 1 by the applied field, traveling across the spacer layer into layer 3, and contributing to the current in layer 3 before getting scattered in that layer. Therefore, for GMR to arise, the electron mean free path in the spacer layer must be long compared to its thickness.

Semiclassical Theory of GMR for Real Materials

Quantitative comparison between theory and experiment requires the theory to go beyond the FERPS model and use real band structures. However, for the most part, quantum coherence effects such as quantum well states and other quantum interference effects are rarely apparent in GMR measurements. The reason for this may lie in the fact that the wavelengths of the Fermi energy electronic states in transition and noble metals are comparable to atomic sizes and therefore comparable to the fluctuations in layer thicknesses in typical polycrystalline sputtered films. For this reason, a full quantum mechanical theory for GMR is usually not necessary, although this perspective may change if film quality improves significantly or if some of the layers only have Fermi energy electron states with long wavelengths.

In this section we will follow a semiclassical approach. The electrons are assumed to behave like classical particles within the context of transport, except that they obey Fermi statistics (which implies that it is the Fermi energy electrons that are important for transport) and that the relation between electron energy and momentum and the transmission and reflection probabilities at interfaces are calculated using quantum mechanics. The quantum mechanical parts of the calculation are performed assuming equilibrium. The transport part is calculated using the Boltzmann transport equation.

Semiclassical Boltzmann Transport Equation

The electron distribution function, $f_s(\mathbf{k}, \mathbf{r}, t)$, is defined as the number of electrons with given values of wave vector $\mathbf{k}$ and spin s, at position $\mathbf{r}$ and time t, a seven-dimensional function (for each spin) measured in dimensionless units. In the absence of applied fields, the electrons are at equilibrium, and the distribution function is the equilibrium distribution function $f_0(E_{s\mathbf{k}}) = [1 + \exp(E_{s\mathbf{k}}/k_BT)]^{-1}$, where the band energy $E_{s\mathbf{k}}$ is measured from the Fermi energy. If an electric field is applied, the distribution function will change, and if the field is not too large, the system will reach a new steady state. The total change in the distribution function (which vanishes in steady state) will consist of contributions from drift, field, and scattering,

$$\frac{df}{dt} = 0 = \left.\frac{\partial f}{\partial t}\right|_{\text{drift}} + \left.\frac{\partial f}{\partial t}\right|_{\text{field}} + \left.\frac{\partial f}{\partial t}\right|_{\text{momentum-scattering}} + \left.\frac{\partial f}{\partial t}\right|_{\text{spin-flip-scattering}}. \tag{54}$$

In this equation, the drift term describes the rate of change of the distribution function due to the movement of electrons caused by their velocity; the field term describes the rate of change of the distribution function due to the acceleration of the electrons caused by the applied external field; the momentum scattering term describes the change in the distribution function due to the scattering of electrons by the imperfections in the lattice which change their momentum, but not their spin; and the spin-flip scattering term describes the change in the distribution function due to scattering processes which change spin.

From the definition of each term, we have the following for the rate of change of f_s:

$$\left.\frac{\partial f_s}{\partial t}\right|_{\text{drift}} = \mathbf{v}(\mathbf{k}) \cdot \nabla f_s(\mathbf{r}, \mathbf{k}) \tag{55}$$

$$\left.\frac{\partial f_s}{\partial t}\right|_{\text{field}} = \frac{\partial \mathbf{k}}{\partial t} \cdot \nabla_k f_s(\mathbf{r}, \mathbf{k}) = \frac{-e}{\hbar} \varepsilon \cdot \nabla_k f_s(\mathbf{r}, \mathbf{k}) \tag{56}$$

$$\left.\frac{\partial f_s}{\partial t}\right|_{\text{momentum-scattering}} = \sum_{\mathbf{k}'} P_{\mathbf{k}\mathbf{k}'}[f_s(\mathbf{r}, \mathbf{k}') - f_s(\mathbf{r}, \mathbf{k})] \tag{57}$$

$$\left.\frac{\partial f_s}{\partial t}\right|_{\text{spin-flip-scattering}} = \sum_{\mathbf{k}'} P^{sf}_{\mathbf{k}\mathbf{k}'}[f_{-s}(\mathbf{r}, \mathbf{k}') - f_s(\mathbf{r}, \mathbf{k})] \tag{58}$$

Equation 56 uses Newton's second law $\left(\dot{\mathbf{p}} = \hbar\dot{\mathbf{k}} = -e\mathcal{E}\right)$ and the notation ∇_k to indicate a gradient in reciprocal space.

The effect of the field, $\mathcal{E}$, on the steady-state distribution function, $f_s(\mathbf{r}, \mathbf{k})$, is to cause deviations from the equilibrium distribution that are limited to the vicinity of the Fermi energy,

$$f_s(\mathbf{r}, \mathbf{k}) = f_0 - \frac{\partial f_0(E_{s\mathbf{k}} - \mu_0)}{\partial E_{s\mathbf{k}}} g_s(\mathbf{r}, \mathbf{k}). \tag{59}$$

We write $g_s(\mathbf{r}, \mathbf{k})$ as the sum of two parts, one that is independent of $\mathbf{k}$ and one whose $\mathbf{k}$-dependence is such that its average over the Fermi surface vanishes.

$$g_s(\mathbf{r}, \mathbf{k}) = \mu_s(\mathbf{r}) - \mu_0 + g^a_s(\mathbf{r}, \mathbf{k}). \tag{60}$$

We shall see that the second part arises naturally in the solution of the Boltzmann equation for a homogeneous system and that the first part is needed to describe cases such as CPP-GMR systems where there spin density can be different from its equilibrium value.

The field term can be simplified by noting that the explicit factor of $\mathcal{E}$ makes it already first order in the field. Therefore, we need only to retain in $\nabla_k f_s(\mathbf{r}, \mathbf{k})$ the lowest nonvanishing order in $\mathcal{E}$. Thus, $\nabla_k f_s(\mathbf{r}, \mathbf{k}) \approx \nabla_k f_0(E_{s\mathbf{k}} - \mu_0)$. Additional simplification of the field term can be obtained by using

$$\nabla_k f_0(E_{s\mathbf{k}} - \mu_0) = \frac{\partial f_0(E_{s\mathbf{k}} - \mu_0)}{\partial E_{s\mathbf{k}}} \nabla_k E_{s\mathbf{k}} = \frac{\partial f_0(E_{s\mathbf{k}} - \mu_0)}{\partial E_{s\mathbf{k}}} \hbar \mathbf{v}_{s\mathbf{k}}. \tag{61}$$

Using these results, the drift, field, and scattering terms can be written as

$$\left.\frac{\partial f}{\partial t}\right|_{\text{drift}} = -\frac{\partial f_0(E_{s\mathbf{k}} - \mu_0)}{\partial E_{s\mathbf{k}}} \mathbf{v}(\mathbf{k}) \cdot \nabla\left[\mu_s(\mathbf{r}) + g_s^a(\mathbf{r}, \mathbf{k})\right] \tag{62}$$

$$\left.\frac{\partial f}{\partial t}\right|_{\text{field}} = -e \frac{\partial f_0(E_{ks} - \mu_0)}{\partial E_{ks}} \mathcal{E} \cdot \mathbf{v}_{ks} \tag{63}$$

$$\left.\frac{\partial f}{\partial t}\right|_{\text{momentum-scattering}} = \frac{\partial f_0(E_{s\mathbf{k}} - \mu_0)}{\partial E_{s\mathbf{k}}} \frac{g_s^a(\mathbf{r}, \mathbf{k})}{\tau_{sk}} \tag{64}$$

$$\left.\frac{\partial f}{\partial t}\right|_{\text{spin-flip-scattering}} = \frac{\partial f_0(E_{s\mathbf{k}} - \mu_0)}{\partial E_{s\mathbf{k}}} \left[-\mu_{-s}(\mathbf{r}) + \mu_s(\mathbf{r}) + g_s^a(\mathbf{r}, \mathbf{k})\right] \frac{1}{\tau_{sk}^{sf}} \tag{65}$$

Equations 64 and 65 depend on the additional approximations

$$\sum_{k'} P_{\mathbf{k}\mathbf{k}'} \frac{\partial f_0(E_{s\mathbf{k}'} - \mu_0)}{\partial E_{s\mathbf{k}'}} g_s^a(\mathbf{r}, \mathbf{k}') = 0 \tag{66}$$

and

$$\sum_{k'} P_{\mathbf{k}\mathbf{k}'}^{sf} \frac{\partial f_0(E_{-s\mathbf{k}'} - \mu_0)}{\partial E_{-s\mathbf{k}'}} g_{-s}^a(\mathbf{r}, \mathbf{k}') = 0. \tag{67}$$

These are equivalent to assumptions that the momentum and spin-flip scattering probabilities are isotropic since by construction

$$\sum_{k'} \frac{\partial f_0(E_{\pm s\mathbf{k}'} - \mu_0)}{\partial E_{\pm s\mathbf{k}'}} g_{\pm s}^a(\mathbf{r}, \mathbf{k}') = 0. \tag{68}$$

Setting the sum of terms Eqs. 62, 63, 64, and 65 to zero yields

$$\mathbf{v}_{s\mathbf{k}} \cdot \nabla\left[\mu_s(\mathbf{r}) + g_s^a(\mathbf{r}, \mathbf{k})\right] + e\varepsilon \cdot \mathbf{v}_{s\mathbf{k}} - g_s^a(\mathbf{r}, \mathbf{k}) \left(\frac{1}{\tau_{s\mathbf{k}}} + \frac{1}{\tau_{s\mathbf{k}}^{sf}}\right) + \frac{\mu_{-s}(\mathbf{r}) - \mu_s(\mathbf{r})}{\tau_{s\mathbf{k}}^{sf}} = 0. \tag{69}$$

The spatial gradient of the chemical potential can be included in the field term by introducing the electrochemical potential $\overline{\mu}_s(\mathbf{r}) = \mu_s(\mathbf{r}) - eV(\mathbf{r})$ which allows us to write Eq. 69 as

$$\mathbf{v}_{s\mathbf{k}} \cdot \nabla\left[g_s^a(\mathbf{r},\mathbf{k}) + \overline{\mu}_s(\mathbf{r})\right] - \left(\frac{1}{\tau_{s\mathbf{k}}} + \frac{1}{\tau_{s\mathbf{k}}^{sf}}\right) g_s^a(\mathbf{r},\mathbf{k}) - \frac{\overline{\mu}_s(\mathbf{r}) - \overline{\mu}_{-s}(\mathbf{r})}{\tau_{s\mathbf{k}}^{sf}} = 0. \tag{70}$$

If we multiply Eq. 70 by $\partial f_0(E_{s\mathbf{k}} - \mu_0)/\partial E_{s\mathbf{k}}$ and average over the Brillouin zone, the terms proportional to $\mathbf{v}_{s\mathbf{k}}\overline{\mu}_s$ and to $g_s^a(\mathbf{r}, \mathbf{k})$ average to zero leaving

$$\sum_k \frac{\partial f_0(E_{s\mathbf{k}} - \mu_0)}{\partial E_{s\mathbf{k}}} \left[\mathbf{v}_{s\mathbf{k}} \cdot \nabla g_s^a(\mathbf{r},\mathbf{k}) + \frac{\overline{\mu}_s(\mathbf{r}) - \overline{\mu}_{-s}(\mathbf{r})}{\tau_{s\mathbf{k}}^{sf}}\right] = 0. \tag{71}$$

But this is just the Valet-Fert equation related to the continuity equation, Eq. 30, because

$$\nabla \cdot \mathbf{J}_s = \frac{e}{V} \sum_k \frac{\partial f_0(E_{s\mathbf{k}} - \mu_0)}{\partial E_{s\mathbf{k}}} \mathbf{v}_{s\mathbf{k}} \cdot \nabla g_s^a(\mathbf{r},\mathbf{k}) = -eN_s \frac{\overline{\mu}_s(\mathbf{r}) - \overline{\mu}_{-s}(\mathbf{r})}{\tau_{s\mathbf{k}}^{sf}}. \tag{72}$$

Similarly, if we multiply Eq. 70 by $(v_{s\mathbf{k}x} \partial f_0(E_{s\mathbf{k}} - \mu_0)/\partial E_{s\mathbf{k}})$ and sum over the Brillouin zone, the terms that survive give

$$\sum_k \frac{\partial f_0(E_{s\mathbf{k}} - \mu_0)}{\partial E_{s\mathbf{k}}} v_{s\mathbf{k}x} g_s^a(\mathbf{r},\mathbf{k}) \left(\frac{1}{\tau_{s\mathbf{k}}} + \frac{1}{\tau_{s\mathbf{k}}^{sf}}\right) = \sum_k \frac{\partial f_0(E_{s\mathbf{k}} - \mu_0)}{\partial E_{s\mathbf{k}}} v_{s\mathbf{k}x}^2 \frac{\partial \overline{\mu}_s}{\partial x}. \tag{73}$$

If we assume that the scattering rates are uniform over the Fermi surface or (more realistically) that their inverse can be replaced by a suitable average lifetime, Eq. 73 yields the other ("Ohm's law") Valet-Fert equation,

$$J_{sx} = \frac{e}{V} \sum_k \frac{\partial f_0(E_{s\mathbf{k}} - \mu_0)}{\partial E_{s\mathbf{k}}} v_{s\mathbf{k}x} g_s^a(\mathbf{r},\mathbf{k}) \approx \frac{e}{V} \sum_k \frac{\partial f_0(E_{s\mathbf{k}} - \mu_0)}{\partial E_{s\mathbf{k}}} v_{s\mathbf{k}x}^2 \frac{\partial \overline{\mu}_s}{\partial x} \left(\frac{1}{\tau_{s\mathbf{k}}} + \frac{1}{\tau_{s\mathbf{k}}^{sf}}\right)^{-1}. \tag{74}$$

Assuming cubic symmetry, we can write this as

$$\mathbf{J}_s = \frac{\sigma_s}{e} \nabla \overline{\mu}_s(\mathbf{r}), \tag{75}$$

where σ_s is given by the usual expression for the conductivity,

$$\sigma_s = \frac{e^2}{3V} \sum_k \frac{-\partial f_0(E_{s\mathbf{k}} - \mu_0)}{\partial E_{s\mathbf{k}}} v_{s\mathbf{k}}^2 \left(\frac{1}{\tau_{s\mathbf{k}}} + \frac{1}{\tau_{s\mathbf{k}}^{sf}}\right)^{-1}. \tag{76}$$

These are just the Valet-Fert expressions that we found by more heuristic approach in section "Spin-Flip Scattering and the Drift-Diffusion Model" with a slightly modified expression for the spin-dependent electron lifetime.

All of the equations in this section have been obtained for a homogeneous system in which spatial changes in the electronic structure are ignored. In applications, the assumption is made (often tacitly) that the electron mean free path is much shorter than the layer thickness. This assumption may be reasonable for some materials and structures.

An additional feature is often added to CPP-GMR models that employ Valet-Fert theory, namely, the use of an additional spin-dependent interfacial resistance. This is typically assumed to result from a thin intermixed interfacial layer, but could also result from a spin-dependent voltage drop resulting from partial reflection of electrons at the interface as discussed in the next section.

Boltzmann Equation for Current-in-Plane Geometry

If the system is composed of layers of different materials stacked along the z-direction, it is often a good approximation to assume that we have two-dimensional periodicity within each layer. If the layers are not too thin, we may also assume that within each layer, we can use the electron dispersion relation appropriate to that material in bulk. We would, of course, have to worry about obtaining the correct relative placement of the energy bands because, in general, when two materials are brought together, a dipole layer forms at the interface to balance the electrochemical potentials and allow the materials to have their correct Fermi energies far from the interfaces.

These approximations lead, then, to a model in which the band energies, $E_{ins\mathbf{k}}$, and velocities, $\mathbf{v}_{ins\mathbf{k}}$, within each layer are assumed to be those for a perfect (infinite) crystal. Here, an additional index, i, has been added to label the layer. The layers are separated by thin, interfacial regions that can be described by transmission and reflection probabilities as we shall show in a later section.

In this section we shall assume that the materials are homogeneous in the x and y directions but that they vary (different materials, interfaces, boundaries, etc.) in the z-direction. Because we have boundaries and interfaces, the distribution function will vary with z and will satisfy Eq. 70 specialized to our layered geometry,

$$\left[v_{izs\mathbf{k}}\frac{\partial}{\partial z}+\frac{1}{\tau_{is}}\right]g_{is}(z,\mathbf{k})=-e\mathbf{v}_{is\mathbf{k}}\cdot\mathcal{E}. \tag{77}$$

In Eq. 77, we have neglected the $\mathbf{k}$-dependence of the lifetimes, and the "scattering-in" term. We assume that the electric field is applied perpendicular to the z-direction which yields the important simplification that the electric field is uniform so that (at least in the absence of spin-orbit coupling) we do not have to worry about spatially varying spin-dependent chemical potentials.

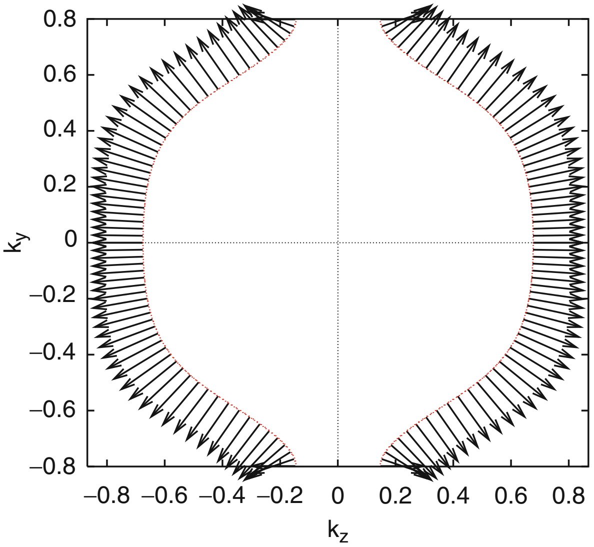

Fig. 4 Cut through the $k_x = 0$ plane of the Fermi surface of copper. The *arrows* indicate the magnitude and direction of the electron velocity. k_y and k_z are given in units of inverse Bohr radii (1.89 Å^{-1}). The k_y direction here is the (111) direction with respect to the conventional cubic axes

The current density, however, will be z-dependent and is given by

$$\mathbf{J}_i(z) = \frac{e}{V}\sum_{s\mathbf{k}} \mathbf{v}_{is\mathbf{k}} g_{is}(z,\mathbf{k})\delta(E_{is\mathbf{k}} - \mu). \tag{78}$$

In Eq. 78 we assume that the temperature is low enough that we can replace the energy derivative of the Fermi function with a delta function. In evaluating the sum over $\mathbf{k} = k_x, k_y, k_z$, we can take advantage of delta function in this layered geometry by converting the sum over k_z into an integral, i.e., $\sum_{k_z} = L\int dk_z/(2\pi)$. Then we can perform the integral over k_z (for fixed $\mathbf{k}_{\|} = k_x,\ k_y$) using the δ-function (suppressing the layer index, i) as

$$\int dk_z \mathbf{v}_{s\mathbf{k}_{\|}k_z} g_s\left(z, \mathbf{k}_{\|}k_z\right)\delta\left(E_{s\mathbf{k}_{\|}k_z} - \mu\right) = \sum_n \frac{g_{ns}\left(z,\mathbf{k}_{\|}\right)\mathbf{v}_{ns}\left(\mathbf{k}_{\|}\right)}{\hbar\left|v_{zns}\left(\mathbf{k}_{\|}\right)\right.}|. \tag{79}$$

Equation 79 requires some explanation. Consider Figures 4 and 5 which depict calculated cuts through the Fermi surfaces of Cu and Co, respectively. Imagine that we are integrating over k_z for arbitrary specified values of k_x and k_y. It is clear from these examples that as we vary k_z from one side of the Brillouin zone to the other, we will pass through the Fermi surface $2n$ times. For Figure 4 and the left panel of Fig. 5, n is one for the chosen value of k_x and any value of k_y. For the right panel of Fig. 5, n will depend on the value k_y for which the integration over k_z is being

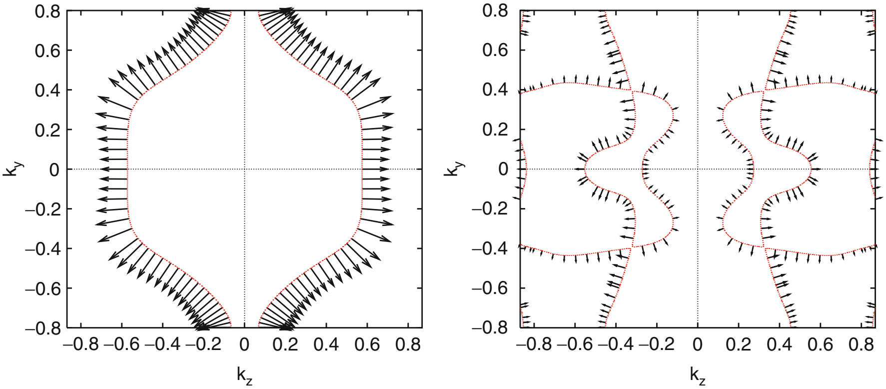

Fig. 5 Cuts through the $k_x = 0$ plane of the majority (*left panel*) and minority (*right panel*) Fermi surfaces of cobalt. The arrows representing the velocities are drawn to the same scale as for copper in Fig. 4 k_y and k_z are given in units of inverse Bohr radii

performed. When k_z crosses the Fermi surface, the argument of the delta function passes through zero. As it passes through zero, we have

$$E_{s\mathbf{k}_{\|}k_z} \approx \mu + \frac{\partial E_{s\mathbf{k}_{\|}k_z}}{\partial k_z}\left(k_z - k_z^{n\pm}\right) = \mu + \hbar v_{zns}\left(\mathbf{k}_{\|}\right)\left(k_z - k_z^{n\pm}\right) \tag{80}$$

where $k_z^{n\pm}$ indicates the value of $k_z(\mathbf{k}_{\|})$ on the nth sheet of the Fermi surface and the ± indicates whether the z-component of the Fermi velocity at this point is positive or negative.

Using Eq. 79 in Eq. 78, we get

$$\mathbf{J}(z) = -\frac{e}{2\pi A}\sum_{ns\mathbf{k}_{\|}} \frac{g_{ns}\left(z,\mathbf{k}_{\|}\right)\mathbf{v}_{ns}\left(\mathbf{k}_{\|}\right)}{\hbar|v_{zns}\left(\mathbf{k}_{\|}\right)}|. \tag{81}$$

It is important to note that for every value of $\mathbf{k}_{\|}$ and n, there will be two states one for which $v_z > 0$ and another with $v_z < 0$. This is true even if the Fermi surface does not have mirror symmetry around the plane $k_z = 0$, as occurs, for example, in fcc Eq. 111. Using this result, we can write Eq. 81 as

$$J_z(z) = -\frac{e}{2\pi A\hbar}\sum_{ns\mathbf{k}_{\|}} \left[g_{ns}^{+}\left(z,\mathbf{k}_{\|}\right) - g_{ns}^{-}\left(z,\mathbf{k}_{\|}\right)\right], \tag{82}$$

where the superscript +(−) indicates the Bloch state with $v_{nsz}^{+}\left(\mathbf{k}_{\|}\right) > 0$ and $\left(v_{nsz}^{-}\left(\mathbf{k}_{\|}\right) < 0\right)$ and the notation $g_{ns}^{\pm}\left(z,\mathbf{k}_{\|}\right)$ stands for $g_{ns}\left(z,\mathbf{k}_{\|},k_z^{n\pm}\right)$.

Boundary Conditions on Interfaces

To uniquely determine the solution to the Boltzmann equation, we need a proper set of boundary conditions. For layered systems electrons traveling in the +z direction satisfy a different boundary condition from those traveling in the $-z$ direction. This was first worked out for single-layer films by Fuchs [14], and the generalization to multilayers [11, 13] is relatively straightforward.

In most cases, the transmission and reflection on the interfaces are coherent, and the spin-flip scattering is also negligible. Therefore, in the discussion of the boundary conditions, we temporarily drop the spin index, s, but add the layer index, i. The boundary conditions on $g_n^{\pm}\left(z, \mathbf{k}_{\|}\right)$ are obtained by requiring particle conservation at each of the interfaces. Since $g_{in}^{+}\left(z, \mathbf{k}_{\|}\right)$ and $g_{in}^{-}\left(z, \mathbf{k}_{\|}\right)$ represent the distribution functions in layer i for electrons traveling in the +z and $-z$ directions, respectively, we can express the relationships between the distribution functions in layers i and $i + 1$ (with interface at z_i) in terms of the transmission $\left(T_i^{++}, T_i^{--}\right)$ and reflection $\left(T_i^{+-}, T_i^{-+}\right)$ probabilities of the interfaces. We use a convention illustrated in Figure 6 in which, for example, $T_i^{+-}(\mathbf{k}, \mathbf{k}')$ is the probability for a $-z$ going electron in Bloch state $\mathbf{k}'$ incident on interface i to leave the interface going in the +z direction in Bloch state $\mathbf{k}$. Consider the flux of electrons leaving this interface traveling in the +z direction (in layer $i + 1$), $\sum_{n, \mathbf{k}_{\|}} g_{i+1, n}^{+}\left(z\mathbf{k}_{\|}\right)$. This flux is the sum of the transmitted flux of +z going electrons from layer i and the reflected flux from those electrons originally traveling in the $-z$ direction in layer $i + 1$. A similar flux conservation argument relates the $-z$ going electron flux leaving the interface to the incoming fluxes in the two layers,

Fig. 6 Convention for the transmission and reflection probabilities

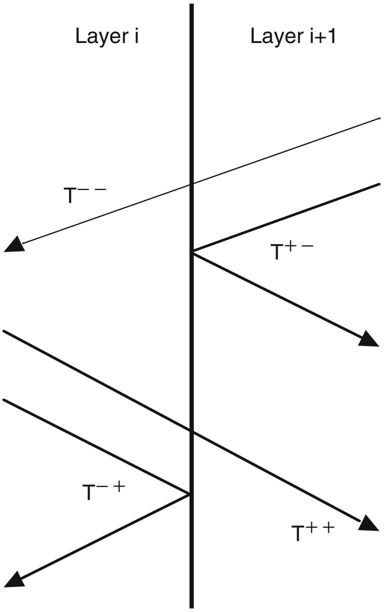

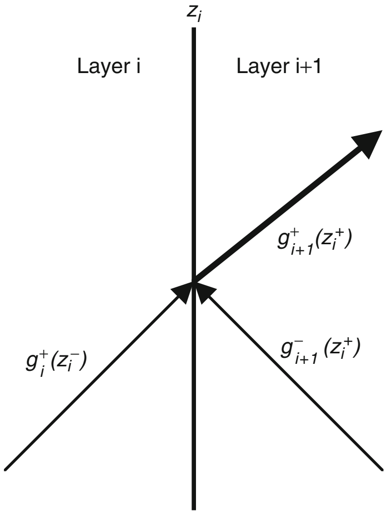

Fig. 7 The *right*-going beam in layer $i + 1$, g^+_{i+1}, is the sum of the reflected part of the *left*-going beam in that layer, g^-_{i+1}, and the transmitted part of the *right*-going beam in layer i, g_i^+

$$\begin{aligned}
g^+_{i+1,n}\left(z_i^+,\mathbf{k}_{\|}\right) &= \sum_{n',\mathbf{k}'_{\|}}^{N_R} T_i^{+-}\left(n\mathbf{k}_{\|},n'\mathbf{k}'_{\|}\right) g^-_{i+1,n'}\left(z_i^+,\mathbf{k}'_{\|}\right)\\
&\quad+\sum_{n',\mathbf{k}'_{\|}}^{N_L} T_i^{++}\left(n\mathbf{k}_{\|},n'\mathbf{k}'_{\|}\right) g^+_{in'}\left(z_i^-,\mathbf{k}'_{\|}\right)\\
g^-_{in}\left(z_i^-,\mathbf{k}_{\|}\right) &= \sum_{n',\mathbf{k}'_{\|}}^{N_L} T_i^{-+}\left(n\mathbf{k}_{\|},n'\mathbf{k}'_{\|}\right) g^+_{in'}\left(z_i^-,\mathbf{k}'_{\|}\right)\\
&\quad+\sum_{n',\mathbf{k}'_{\|}}^{N_R} T_i^{--}\left(n\mathbf{k}_{\|},n'\mathbf{k}'_{\|}\right) g^-_{i+1,n'}\left(z_i^+,\mathbf{k}'_{\|}\right)
\end{aligned}\quad . \qquad (83)$$

Here N_L and N_R denote the number of states on the left or right of the interface, respectively, for a given value of $k_{|}|'$. If we assume that the layers have two-dimensional periodicity, so that the momentum parallel to the interface is conserved on transmission or reflection, the boundary conditions become

$$\begin{aligned}
g^+_{i+1,n}\left(z_i^+,\mathbf{k}_{\|}\right) &= \sum_{n'}^{N_R} T_i^{+-}(n,n') g^-_{i+1,n'}\left(z_i^+,\mathbf{k}_{\|}\right)\\
&\quad+\sum_{n'}^{N_L} T_i^{++}(n,n') g^+_{in'}\left(z_i^-,\mathbf{k}_{\|}\right)\\
g^-_{in}\left(z_i^-,\mathbf{k}_{\|}\right) &= \sum_{n'}^{N_L} T_i^{-+}(n,n') g^+_{in'}\left(z_i^-,\mathbf{k}_{\|}\right)\\
&\quad+\sum_{j'}^{N_R} T_i^{--}(n,n') g^-_{i+1,n'}\left(z_i^+,\mathbf{k}_{\|'}\right)
\end{aligned}\quad . \qquad (84)$$

Fig. 8 Transmission probabilities of copper electrons incident on majority cobalt for a cut through the Fermi surface with $k_y = 0$. The Fermi surface of copper and majority cobalt are also shown

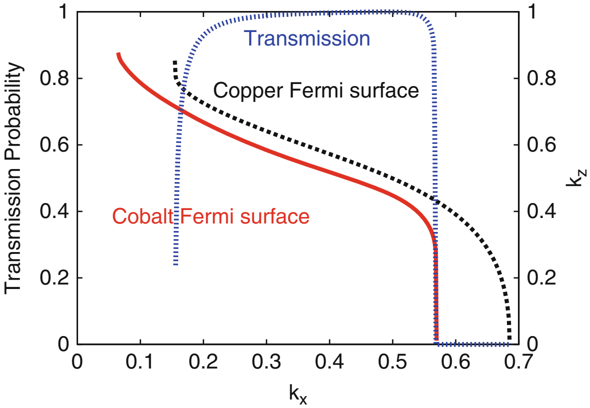

Fig. 9 Transmission probabilities of copper electrons incident on minority cobalt for a cut through the Fermi surface with $k_y = 0$. The Fermi surface of minority cobalt is also shown. Note that the transmission probability goes to zero if the velocity of the state receiving the electrons goes to zero. This is a consequence of flux conservation

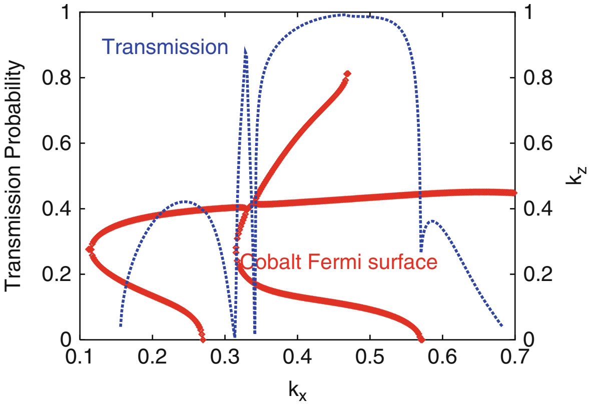

The first of these relations is shown pictorially in Figure 7. The transmission and reflection matrices can be calculated from the underlying electronic structure of the layers and their interface [16]. Figures 8 and 9 show the transmission and reflection probabilities for Bloch waves in copper incident on cobalt. The transmission and reflection probabilities conserve electron flux. Thus, considering incident left- and right-going waves of unit flux, respectively, we can derive the following conservation rules,

$$\begin{aligned} \sum_n^{N_R} T_i^{++}(n,n') + \sum_n^{N_L} T_i^{-+}(n,n') &= 1 \\ \sum_n^{N_L} T_i^{--}(n,n') + \sum_n^{N_R} T_i^{+-}(n,n') &= 1, \end{aligned} \tag{85}$$

and considering unit left- and right-going fluxes leaving the interface, we obtain

$$\begin{aligned}
&\sum_{n'}^{N_L} T_i^{++}(n,n') + \sum_{n'}^{N_R} T_i^{+-}(n,n') = 1 \\
&\sum_{n'}^{N_R} T_i^{--}(n,n') + \sum_{n'}^{N_L} T_i^{-+}(n,n') = 1.
\end{aligned} \tag{86}$$

CIP GMR Using Realistic Electronic Structure

CIP GMR arises from the nonlocal nature of electrical conduction. A necessary requirement for CIP GMR is that the electron mean free path be at least comparable to the thicknesses of the layers. One contribution to CIP GMR can be thought of as an effect similar to the effect of a boundary decreasing the conductivity. Consider a three-layer system, e.g., a layer of copper sandwiched between two layers of cobalt. Suppose that copper and cobalt matched perfectly in the majority channel. Then the majority electrons, when the moments of the two cobalt layers are aligned, would effectively see a film thickness equal to the sum of the thicknesses of the three layers while the minority electrons would tend to be confined within the individual layers because of the changes in electronic structure at the interfaces. When the moments are anti-aligned, however, both of the spin channels would see effectively two layers. This causes a difference in the total current and the giant magnetoresistance.

In fact, of course, as indicated in Figures 4, 5, and 8, there is a difference between cobalt and copper in the majority channel. The copper majority Fermi surface is larger than that of cobalt. It holds 0.5 electrons while that of cobalt holds only 0.3. A cut through the Fermi surfaces of copper and majority cobalt is shown in Figure 8. The z-direction (perpendicular to the layers) is toward the top of the figure. The directions perpendicular to this direction are in the plane of the layers. If the interfaces are smooth on an atomic scale, then the component of the momentum parallel to the interface ($\mathbf{k}_{||}$) does not change on reflection or refraction at an interface. Thus, from Figure 8, it is clear that there are values of $\mathbf{k}_{||}$ for which states exist in the copper but not in the cobalt. This means that these states cannot refract into the cobalt; they must reflect back into the copper. This can lead to a significant contribution to the GMR if the interface is sufficiently smooth because some of the majority electrons can be "trapped" inside the copper where the resistance is significantly lower for both spin channels than for cobalt. This "trapping" of the electrons inside the copper layer is analogous to the trapping of light waves within a waveguide [17]. Note from Fig. 14 that interfacial disorder is relatively ineffective in reducing the specular reflection for values of $k_{||}$ where total reflection occurs.

A calculation for the current density in a CIP cobalt|copper|cobalt spin valve using realistic electronic structures is shown in Figures 10 and 11. Figure 10 shows the majority and minority currents for both parallel (↑↑, ↓↓) and antiparallel (↑↓, ↓↑) alignments. In this example, the scattering rate in the copper is chosen to give the copper a resistivity of 3 μΩ cm, a typical value for sputter-deposited copper films at room temperature. The scattering rates for cobalt were chosen to give it a resistance of 15 μΩ cm which is also typical of sputtered films. A much higher scattering rate

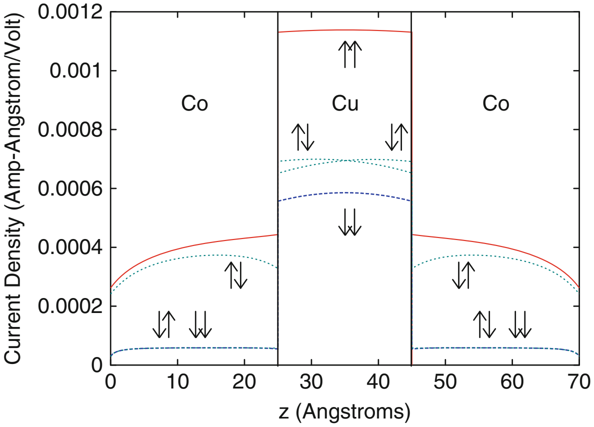

Fig. 10 Current densities for CIP Co|Cu|Co spin valves. The scattering rates correspond to bulk resistivities of 3 μΩ cm for copper and 15 μΩ cm for cobalt with the majority lifetime ten times longer than the minority lifetime for cobalt

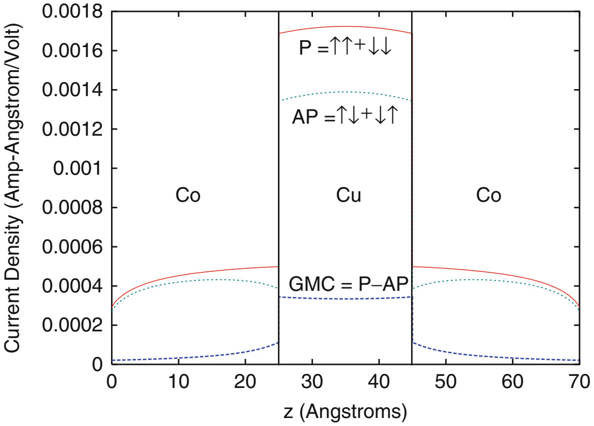

Fig. 11 Current densities for parallel alignment, antiparallel alignment, and difference or giant magnetoconductance for a CIP Co-Cu spin valve

was chosen for the minority than for the majority cobalt. It can be seen that the current density is significantly higher in the copper than in the cobalt. It can be seen from Figure 11 that the largest contributions to the giant magnetoconductance arise from the copper spacer layer indicating the importance of the channeling effect. Comparison of calculated and measured values of GMR for a series of cobalt-copper spin valves with different thicknesses of the cobalt layers indicated the existence of important contributions to GMR from both the channeling effect and from the differences in bulk scattering rates for the majority and minority channels of cobalt (Fig. 11).

Boltzmann Equation for CPP

When the system is inhomogeneous in the direction in which the field is applied, there will be accumulation of spin and charges near the interfaces between the layers. Leaving aside possible spin accumulation for the time being, charge accumulation can be easily illustrated through the example of a system with a local but

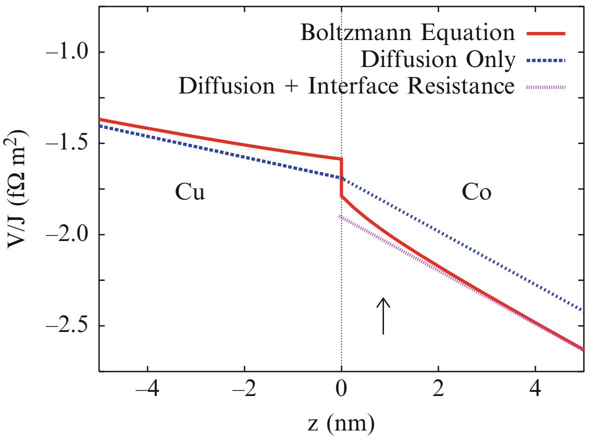

Fig. 12 Chemical potential divided by current density for copper-cobalt majority interface

spatially varying conductivity $\sigma(z)$ that depends on z, the direction which sustains a current, J. The current density is related to the local electric field through the conductivity,

$$J(z) = \sigma(z)\mathcal{E}(z). \tag{87}$$

In steady state, $J(z)$ must be independent of z if charge is to be conserved. Thus, the local field, $E(z)$, must vary as $J/\sigma(z)$. We can think of this local field as arising from an applied field together with the fields due to the inhomogeneous distribution of electrons that is set up by the current passing through the sample. The case with both charge and spin accumulation was treated in section "Spin-Flip Scattering and the Drift-Diffusion Model" using a model in which the electronic structure did not change from one layer to the next.

Here we extend that model for the case in which the electronic structure of the layers may differ. We begin with the Boltzmann equation, Eq. 70, specialized to our geometry (Fig. 12),

$$v_{zs\mathbf{k}}\frac{\partial}{\partial z}\left[g_s^a(z,\mathbf{k}) + \overline{\mu}_s(z)\right] - \left(\frac{1}{\tau_s} + \frac{1}{\tau_s^{sf}}\right)g_s^a(z,\mathbf{k}) - \frac{\overline{\mu}_s(z) - \overline{\mu}_{-s}(z)}{\tau_s^{sf}} = 0. \tag{88}$$

Just as in section "Semiclassical Boltzmann Transport Equation," we can average this equation over the Fermi surface obtaining

$$\frac{\partial J_{zs}(z)}{\partial z} = -eN_s\frac{\overline{\mu}_s - \overline{\mu}_{-s}}{\tau_s^{sf}}, \tag{89}$$

while averaging after multiplying by $v_{zs\mathbf{k}}$ gives

$$J_{zs}(z) = \frac{\sigma_s}{e}\frac{\partial\overline{\mu}_s}{\partial z}. \tag{90}$$

Fig. 13 Chemical potential divided by current density for copper-cobalt minority interface

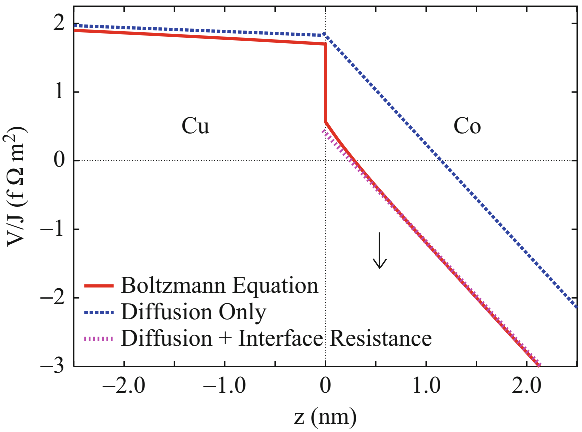

Just as in section "Semiclassical Boltzmann Transport," these two Valet-Fert equations can be solved within each layer. However, the boundary conditions that are used to connect solutions in different layers are now determined by the transmission and reflection expressions derived in section "Boundary Conditions on Interfaces." As a consequence, it is not sufficient to calculate only the spin-dependent currents and chemical potentials. It seems to be necessary to calculate the entire distribution function. An important point that must be kept in mind in applying the boundary conditions is that they must refer to the entire deviation function, not simply the anisotropic part.

The Boltzmann equation together with the matching conditions at the boundaries can be solved by an iterative process [18]. Figures 12 and 13 show the calculated electrochemical potential, $\overline{\mu}$, for the majority and minority channels in the vicinity of a copper-cobalt interface. The scattering rates are similar to those used for the CIP calculations; the bulk resistivity of the copper is approximately 3 μΩ cm and that of the cobalt is approximately 15 μΩ cm with a scattering rate about 15 times higher for minority cobalt than for majority cobalt. The electrochemical potential has been divided by the current density so that the plots yield $\int dx \rho_s(z)$. Without incorporating the actual band structures of the copper and cobalt in the Boltzmann equation, one would simply obtain a straight line for each layer with the slope of the line being its resistivity. Using the actual band parameters in the Boltzmann equation leads to two main differences: (1) There is a discontinuity in the chemical potential at the interface which is equivalent to an interfacial resistance. This interfacial resistance is not due to intermixing or additional scattering at the interface (although this effect can be included in the model if desired) but to the mismatch of the bands across the interface which causes some of the electrons incident on the interface to be reflected. (2) There are exponential terms in the electrochemical potential in the vicinity of the interface that decay at a rate comparable to the component of the mean free path perpendicular to the layers.

The effect of these terms can be included as an additional interfacial resistance that is added to the discontinuous contribution just described as is indicated in the dotted lines of Figures 12 and 13. If this is done, however, it must be taken into consideration that this additional contribution depends on the environment of the interface, e.g., the proximity of other interfaces. The calculated interfacial resistances are comparable to those observed [5] in cobalt-copper multilayers at low temperature.

Diffuse Interfacial Scattering

If the interface is disordered, the flux conservation rules must be extended to include the scattering of electrons between different values of $\mathbf{k}_{\|}$. Diffuse scattering by interfaces and surfaces can be treated phenomenologically by including a specularity parameter S_i for each interface so that Eq. 84 becomes

$$\begin{aligned} g_{i+1}^{+,j}\left(z_i^+,\mathbf{k}_{\|}\right) &= S_i\left[\sum_{j'}^{N_R} T_i^{+-}(j,j')\,g_{i+1}^{-,j'}\left(z_i^+,\mathbf{k}_{\|}\right)\right. \\ &\qquad \left.+\sum_{j'}^{N_L} T_i^{++}(j,j')\,g_i^{+,j'}\left(z_i^-,\mathbf{k}_{\|}\right)\right] \\ g_i^{-,j}\left(z_i^-,\mathbf{k}_{\|}\right) &= S_i\left[\sum_{j'}^{N_L} T_i^{-+}(j,j')\,g_i^{+,j'}\left(z_i^-,\mathbf{k}_{\|}\right)\right. \\ &\qquad \left.+\sum_{j'}^{N_R} T_i^{--}(j,j')\,g_{i+1}^{-,j'}\left(z_i^+,\mathbf{k}_{\|'}\right)\right]. \end{aligned} \tag{91}$$

The value of S_i is between zero and one. For purely specular scattering, i.e., a perfectly clean interface where $\mathbf{k}_{\|}$ is always conserved, $S_i = 1$. In the other extreme, for completely diffuse scattering $S_i = 0$. Although Eq. 91 is technically consistent with the spirit of the lifetime approximation, because it neglects all scatter-in terms when $S_i < 1$, it does not conserve flux. This does not cause a problem for CIP when there is no net current flowing perpendicular to the interface and the current parallel to the interface is still conserved. For CPP a scatter-in term has to be added to keep the flux constant across the interface. There is no clear choice for the form of the scatter-in term. In the case of isotropic scattering, one can add a term proportional to the difference in the chemical potential on both sides of the interface.

The constant specularity parameter approach to diffuse scattering is not very accurate and may not even be physical [11]. A model system in which there are random point scatterers at the interface between two free-electron regions can be solved in closed form in the weak scattering limit [19]. The result is a specularity function that is strongly dependent on $\mathbf{k}_{\|}$ and that is quite different for transmission and reflection. The specularity function for transmission in this model is

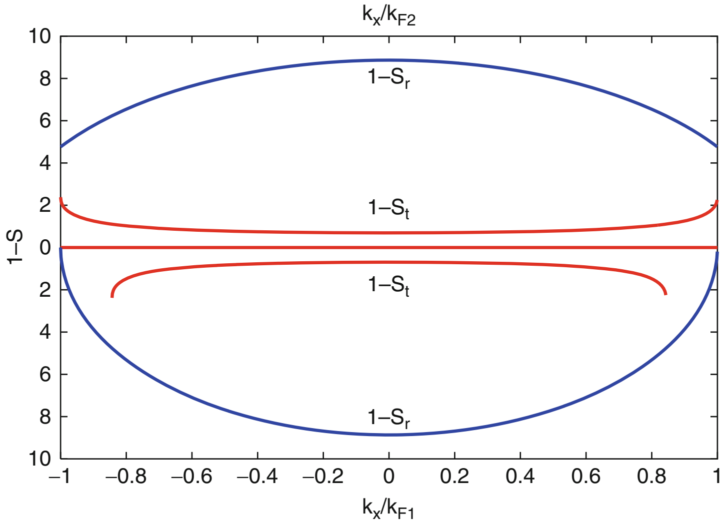

Fig. 14 $1 - S_t$ and $1 - S_r$ in the effective mass approximation. The Fermi momentum, k_{F1} corresponds to 0.5 electrons per spin channel (e.g., as in Cu) while k_{F2} corresponds to 0.3 electrons per spin channel (e.g., as in majority Co). The values of $1 - S_t$ and $1 - S_r$ are measured in terms of the dimensionless parameter $2m_e\gamma n_0 a/\hbar^2$, where α is the lattice constant which is assumed to be fcc

$$S_t\left(\mathbf{k}_{\|}\right) = 1 - \frac{4\pi}{\hbar}\frac{\gamma n_0}{v_z^L\left(\mathbf{k}_{\|}\right) + v_z^R\left(\mathbf{k}_{\|}\right)} \tag{92}$$

where γ is a measure of the interface roughness (γ is defined by the correlation function of the random interfacial potential, $\langle V(\mathbf{r})V(\mathbf{r}')\rangle = \gamma\delta(\mathbf{r} - \mathbf{r}')\delta(z)$), n_0 is the Fermi energy DOS at the interface, and v^L and v^R are the electron velocities on the right and left sides of the interface. Similarly, the specularity function for reflection is

$$S_r\left(\mathbf{k}_{\|}\right) = 1 - \frac{8\pi}{\hbar}\frac{v_z^L\left(\mathbf{k}_{\|}\right)\gamma n_0(0;E)}{\left(v_z^L\left(\mathbf{k}_{\|}\right)\right)^2 - \left(v_z^R\left(\mathbf{k}_{\|}\right)\right)^2}. \tag{93}$$

Note that within this model, interfacial disorder can only decrease the specular transmission, but it can either decrease or enhance the specular reflection depending on the velocities on either side of the interface. Specular transmission remains symmetric in the sense that that transmission from left to right remains the same as from right to left. Specular reflection, however, is no longer symmetric in the presence of a disordered interface.

The specularity parameters calculated from Eqs. 92 and 93 are plotted both as functions of $k_{\|}/k_{F1}$ and $\mathrm{k}_{\|}/k_{F2}$ in Fig. 14, where k_{F1} and k_{F2} are the Fermi wave vectors of the materials on two sides of the interface, respectively. Note that within this model the diffuse scattering vanishes as $k_{\|} \to k_{F1}$. Generally, however, the model predicts the effects of diffuse scattering to be significantly greater for the reflected beam than for the transmitted beam.

Theoretical Approach for Spin-Dependent Tunneling

Julliere Model

The first model used to describe spin-dependent tunneling was proposed by Julliere in 1975 [20]. In this model the spin-dependent tunneling conductance is described in terms of a polarization, P, of electrons "tunneling from ferromagnetic metals,"

$$P = \frac{n^{\uparrow} - n^{\downarrow}}{n^{\uparrow} + n^{\downarrow}}; \tag{94}$$

thus

$$\frac{n^{\uparrow}}{n^{\downarrow}} = \frac{1+P}{1-P}, \tag{95}$$

where $n^{\uparrow}$ and $n^{\downarrow}$ are some kind of the spin-polarized electron "density of states." The tunneling conductance is then assumed to be proportional to the product of these "density of states" from the two electrodes,

$$G_P = C\left(n_1^{\uparrow} n_2^{\uparrow} + n_1^{\downarrow} n_2^{\downarrow}\right) \tag{96}$$

$$G_{AP} = C\left(n_1^{\uparrow} n_2^{\downarrow} + n_1^{\downarrow} n_2^{\uparrow}\right), \tag{97}$$

where the subscripts P and AP indicate the parallel and the antiparallel alignments of the magnetic moments in the two electrodes, 1 and 2 label the two electrodes, and C is a constant independent of the moment alignment. The magnetoconductance is then

$$\frac{G_P - G_A}{G_P} = \frac{\left(n_1^{\uparrow} n_2^{\uparrow} + n_1^{\downarrow} n_2^{\downarrow}\right) - \left(n_1^{\uparrow} n_2^{\downarrow} + n_1^{\downarrow} n_2^{\uparrow}\right)}{n_1^{\uparrow} n_2^{\uparrow} + n_1^{\downarrow} n_2^{\downarrow}} = \frac{2P_1P_2}{1+P_1P_2}. \tag{98}$$

This is the well-known Julliere formula for spin-dependent tunneling. It has been widely used to rationalize measurements of magnetic tunnel junctions, in particular to extract the values of spin polarizations P_1 and P_2 through the measurements of magnetoresistance. However, it is clear that these polarizations are defined in terms of $n^{\uparrow}$ and $n^{\downarrow}$ whose meaning is ambiguous. They cannot be the actual electron density of states at the Fermi energy for ferromagnetic electrodes, where the minority spin has a much greater density of states than the majority spin, opposite of the spin polarization values extracted from tunneling experiments. It may be argued that the definition of the spin polarization parameter should include the tunneling matrix element of the barrier. But then P is no longer a property of the electrode alone. A proper treatment of spin-dependent tunneling must begin from the tunneling theory.

Landauer Formula

Tunneling conductance can be calculated using a very simple but general result due to Landauer [21] which relates the conductance to the probability of a Bloch electron in one of the electrodes being transmitted through the barrier layer to the opposite electrode. To understand the Landauer conductance formula, it is helpful to consider two reservoirs for electrons connected by a sample as shown in Fig. 15. If we imagine the left reservoir, with chemical potential μ_L, to be an emitter of right-going electrons, we can write the current density of those electrons that leave the reservoir on the left and enter the reservoir on the right as

$$J^+ = \frac{e}{(2\pi)^3} \int d^3k v_z^+(\mathbf{k}) f(E - \mu_L) T^+(\mathbf{k}) \tag{99}$$

where

$$T^+(\mathbf{k}) \equiv \sum_{k'} T^{++}(\mathbf{k}, \mathbf{k}') \tag{100}$$

is the transmission probability of an electron at energy E and momentum $\hbar\mathbf{k}$ and z is the direction from reservoir L to reservoir R. In general the scattering within the sample region may not conserve the momentum; thus, the incident wave vector $\mathbf{k}$ and the exit wave vector $\mathbf{k}'$ may not be the same, and the total transmission is calculated by summing over all $\mathbf{k}'$. For ballistic tunneling through epitaxial junctions, the transverse component $\mathrm{k}_{\|}$ is conserved. The group velocity $v_z^+(\mathbf{k}) = (1/\hbar)$ $\partial E/\partial k_z$ which leads to

$$\begin{aligned} J^+ &= \frac{e}{(2\pi)^2} \int_0^\infty k_{\|} dk_{\|} \int_0^\infty dk_z \frac{1}{\hbar} \frac{\partial E}{\partial k_z} f(E - \mu_L) \sum_j T^+(\mathbf{k}, j), \\ &= \frac{e}{2\pi h} \int_0^\infty k_{\|} dk_{\|} \int_0^\infty dE \sum_j T^+\left(k_{\|}, j\right) f(E - \mu_L). \end{aligned} \tag{101}$$

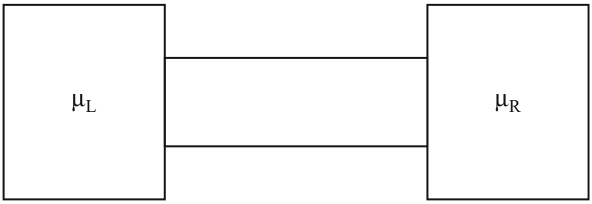

Fig. 15 Two electron reservoirs connected by a conductor

Here, the sum over j is needed because there will, in general, be more than one Bloch state for a given value of $k_{\|}$. A line of reasoning similar to the one that led to Eq. 101 leads to an expression for the current of electrons emitted in the $-z$ direction by the reservoir on the right which enter the reservoir on the left,

$$J^{-} = \frac{e}{2\pi h}\int_0^{\infty} k_{\|}dk_{\|}\int_0^{\infty} dE\sum_j T^{-}\left(k_{\|},j\right)f(E-\mu_R). \tag{102}$$

Assuming time reversal invariance (to apply the time reversal argument rigorously, we should reverse the moment directions as well as the electron directions. If we ignore spin-orbit coupling, however, $T^{+} = T^{-}$ for the individual spin channels), we can equate T^{+} and T^{-}. We further neglect the energy dependence of the transmission probabilities. This allows us to write the net current as

$$J = J^{+} - J^{-} = \frac{e}{2\pi h}\int_0^{\infty} k_{\|}dk_{\|}\int_0^{\infty} dE\sum_j T^{+}\left(k_{\|},j\right)[f(E-\mu_L) - f(E-\mu_R)]. \tag{103}$$

For a small bias voltage and low temperature, the energy dependence of $T^{+}(k_{\|}, J)$ within the transport window $\mu_L < E < \mu_R$ (and a few kT both above and below) can be neglected, and the integral over E can be carried out,

$$\int_0^{\infty} dE[f(E-\mu_L) - f(E-\mu_R)] = -kT\ln\left[\frac{1+e^{-(E-\mu_L)/kT}}{1+e^{-(E-\mu_R)/kT}}\right]\Bigg|_0^{\infty} = \mu_L - \mu_R. \tag{104}$$

$$J = \frac{e}{2\pi h}(\mu_L - \mu_R)\int_0^{\infty} k_{\|}dk_{\|}\sum_j T^{+}\left(k_{\|},j\right). \tag{105}$$

Taking the derivative with respect to $V = (\mu_L - \mu_R)/e$ yields the Landauer conductance formula,

$$G = \frac{e^2}{h}\sum_{k_{\|},j} T^{+}\left(k_{\|},j\right). \tag{106}$$

The physical interpretation of the Landauer conductance formula is that the conductance is given by a sum over the transverse normal modes of the sample ($k_{\|}$ here). The conductance contributed by each normal mode is given by the probability that the electron in that transverse normal mode will be transmitted. Each normal mode contributes a maximum conductance of e^2/h. In addition to its use in describing tunneling, it is also used extensively to describe electron transport through molecules.

Ballistic transport such as described by the Landauer conductance formula neglects electron scattering except for that explicitly included in the transmission probability. As we learned in problem 1, however, a conductor will have a nonzero resistance and a finite conductance even if the electrons are transmitted without scattering because the number of transverse normal modes is finite.

The original Landauer formula has the ratio of transmission probability divided by reflection probability (T/R) where we have only the transmission probability in Eq. 106. It is now usually accepted that this additional factor of $1/R$ is present or not depending on exactly how the measurement is performed, that is, on whether or not one measures current and voltage using the same leads, as is assumed in the derivation here, or whether a separate set of probes is used to determine the voltage across the sample.

Spin-Dependent Tunneling in the Free-Electron Model

Layer-Wise Free-Electron Model

The theory of electron tunneling can be presented cogently in terms of a general electronic structure. It is instructive, however, to have a specific electronic structure in mind. This will allow us to perform calculations that will help us to understand how the theory works in a concrete context. Once the principles are understood, it should be straightforward (if tedious) to apply them to more accurate and detailed representations of the electronic structure.

Given a one electron Hamiltonian, H, and its associated Schrödinger equation, $H_\psi = E_\psi$, various techniques can be used to solve for the wave functions and energy spectrum. Two of the simplest approximations for the electronic structure are the free-electron model and the tight-binding model. In the free-electron model, only the kinetic energy term of the Schrödinger equation is retained. The free-electron model provides a reasonable representation of the energy bands in the vicinity of the Fermi surface of certain metals, notably the alkali metals (e.g., Na, K, Rb, Cs); some of the simple metals such as Al, Zn, and Cd; the conduction bands of some semiconductors; and the noble metals (Cu, Ag, and Au). The free-electron model is not well suited for describing the electronic structure of transition metals except in special cases. One of these cases is the majority conduction bands of Ni and Co. For ferromagnetic Ni and Co, the exchange interaction shifts the majority bands down with respect to the minority bands so that the Fermi energy intersects the majority bands above the d-bands so that the Fermi surface is a nearly closed object resembling a sphere with eight small "necks." The primary justification for our use of the free-electron approximation is that it allows us to perform simple calculations that help us to understand the more complicated systems that are more relevant to experiment.

When two metallic layers are brought into contact, there will typically be a transfer of electrons from one layer to the other. This transfer of charge is necessary to equalize the Fermi levels of the two metals and results in a dipole layer that resides near the interface. A similar charge rearrangement also occurs when a metallic layer is interfaced with an insulator or semiconductor layer. For thick insulator or semiconductors, a Schottky barrier can form that may extend for hundreds of nanometers. The ultrathin insulating barrier layers in magnetic tunnel junctions are typically only a few nanometers thick. Such a thickness is not sufficient to build a Schottky barrier. Nonetheless, there is still an interface dipole layer due to the charge transfer between the metal and the barrier layer. Such effects are neglected in a free-electron model. The change in potential at the interface is simply treated as a step. Since the potential in the Schrödinger equation depends only on z and not on x or y, we can write

$$\left[-\frac{\hbar^2}{2m}\nabla^2 + V(z)\right]\psi(x, y, z) = E\psi(x, y, z).$$

Because of the planar symmetry, we can separate variables by writing $\psi(x, y, z) = X(x)Y(y)Z(z)$. On substitution and division by $\psi(x, y, z)$, we have

$$-\left(\frac{1}{X}\frac{d^2X}{dx^2} + \frac{1}{Y}\frac{d^2Y}{dy^2} + \frac{1}{Z}\frac{d^2Z}{dz^2}\right) = \frac{2m}{\hbar^2}[E - V(z)].$$

The solutions for $X(x)$ and $Y(y)$ are simply $X(x) = \exp(\pm ik_x x)$ and $Y(y) = \exp(\pm ik_y y)$. It would be equally valid to use sines and cosines, but we will use exponentials because we will ultimately establish a correspondence between a wave function proportional to $\exp(ik_x x + ik_y y + ik_z z)$ and a semiclassical electron with momentum $\hbar\mathbf{k}$.

Using the solutions for $X(x)$ and $Y(y)$, our Schrödinger equation becomes

$$-\frac{1}{Z}\frac{d^2Z}{dz^2} = \frac{2m}{\hbar^2}(E - V(z)) - k_x^2 - k_y^2,$$

where k_x and k_y are independent of z. The fact that $\mathbf{k}_{\|} = k_x\hat{x} + k_y\hat{y}$ does not change between layers is called $\mathbf{k}_{\|}$ conservation. It results from our assumption that $V(z)$ depends only on z. If the interfaces between the layers are smooth, the component of the electron's momentum parallel to the interfaces does not change from one layer to the next.

Let us assume that our system consists of layers in the z-direction and that the potential is constant with value within each layer.

$$-\frac{\partial^2}{\partial z^2}Z(z) = \left[\left(\frac{2m}{\hbar^2}\right)(E_F - V_L) - k_x^2 - k_y^2\right]Z(z).$$

The solution within each layer is then trivial, $Z(z) = Ae^{ik_{zL}z} + Be^{-ik_{zL}z}$, where $Z(z) = Ae^{ik_{zL}z} + Be^{-ik_{zL}z}k_{zL} = \sqrt{\left(\frac{2m}{\hbar^2}\right)(E_F - V_L) - k_x^2 - k_y^2}$. Because the x- and y-components of the electron's momentum, k_x and k_y, are conserved at the interfaces between the layers, changes in k_F due to a change in potential as the electron moves between layers, it will be the z-component of the momentum that changes. We will suppress the z subscript on k_z and write $k = \sqrt{k_{FL}^2 - k_x^2 - k_y^2} = k_{FL}\cos\theta$, where $\cos\theta$ is the angle between the electron's momentum and the normal to the layers, i.e., the z-axis. It is easy to forget (and important to remember) in the following, however, that it is the z-component of the momentum that is represented.

One-Dimensional Model for Spin-Dependent Tunneling

A very simple model for spin-dependent tunneling can be derived from a transmission problem through a one-dimensional tunnel barrier for free electrons. Suppose that the wave vectors in three regions of space are k_1 (left lead), $i\kappa$ (barrier region), and k_2 (right lead), then the transmission coefficient for this barrier can be found easily through matching the wave functions and their derivatives across the three regions. We find

$$T = \frac{16 k_1 \kappa k_2 \exp(2\kappa d)}{\{\kappa(k_1 + k_2)[1 + \exp(2\kappa d)]\}^2 + \{(\kappa^2 - k_1 k_2)[1 - \exp(2\kappa d)]\}^2} \tag{107}$$

where d is the barrier thickness. In the limit of $\kappa d \gg 1$, T is simplified to

$$T = \frac{16 k_1 \kappa k_2 \exp(-2\kappa d)}{\left(\kappa^2 + k_1^2\right)\left(\kappa^2 + k_2^2\right)}. \tag{108}$$

In the free-electron model, the two spin channels have different wave vectors, $k_\uparrow = \sqrt{E_F - V_\uparrow}$ and $k_\downarrow = \sqrt{E_F - V_\downarrow}$, at the Fermi level, where $V_\uparrow$–$V_\downarrow$ is the exchange splitting. Thus, the majority conductance for parallel alignment of the moments on opposite sides of the barrier is found from Eqs. 108 and 106 using $k_1 = k_2 = k_\uparrow$, and for the minority conductance $k_1 = k_2 = k_\downarrow$,

$$G_P = 16 \frac{e}{h} \kappa \exp(-2\kappa d) \left[\frac{k_\uparrow^2}{\left(\kappa^2 + k_\uparrow^2\right)^2} + \frac{k_\downarrow^2}{\left(\kappa^2 + k_\downarrow^2\right)^2} \right]. \tag{109}$$

The conductance for antiparallel alignment of the moments is obtained by setting $k_1 = k_\uparrow$, $k_2 = k_\downarrow$,

$$G_{AP} = 32 \frac{e}{h} \kappa \exp(-2\kappa d) \frac{k_\uparrow k_\downarrow}{\left(\kappa^2 + k_\uparrow^2\right)\left(\kappa^2 + k_\downarrow^2\right)}. \tag{110}$$

The tunneling magnetoresistance (TMR), defined as $(G_P - G_{Ap})/G_P$, is given by

$$\frac{G_P - G_{AP}}{G_P} = \frac{2\left(\kappa^2 - k_\uparrow k_\downarrow\right)^2 \left(k_\uparrow - k_\downarrow\right)^2}{\left(\kappa^2 + k_\uparrow k_\downarrow\right)^2 \left(k_\uparrow + k_\downarrow\right)^2 + \left(\kappa^2 - k_\uparrow k_\downarrow\right)^2 \left(k_\uparrow - k_\downarrow\right)^2}. \tag{111}$$

The polarization of the tunneling electrons used in the Julliere model, applied to free electrons, is simply that of the Fermi energy electrons, i.e.,

$$P = \frac{k_\uparrow - k_\downarrow}{k_\uparrow + k_\downarrow}. \tag{112}$$

The TMR given by Eq. 111 cannot be easily reduced into a simple function of P as in the Julliere formula, Eq. 98. However, if we define an effective polarization in place of P, defined as

$$P_{\text{eff}} = P\frac{\kappa^2 - k_\uparrow k_\downarrow}{\kappa^2 + k_\uparrow k_\downarrow}, \tag{113}$$

then the TMR in Eq. 111 becomes

$$TMR = \frac{P_{\text{eff}}^2}{1 + P_{\text{eff}}^2}. \tag{114}$$

This form resembles the original Julliere formula, Eq. 98, and is its generalization to the free-electron model by Slonczewski [22]. However, now the conductance ratio would depend on the type of tunnel junction. Although Slonczewski's generalization does provide a reasonable description of free-electron tunneling through a step barrier, it is not simple to apply to experiment because the effective polarization P_{eff} depends on both the ferromagnet moment alignment and the barrier height and thus cannot be uniquely defined for each material.

Compared to the Julliere model which assumes that the barrier has no effect on the TMR, the Slonczewski model is an improvement and accounts for some of the effects of the barrier layer. However, the assumption of a single decay length for wave functions of both spins in the barrier layer is a severe limitation that still limits the achievable TMR to the spin polarization of the electrodes. An important contribution to the TMR comes from the symmetry-filtering effect of the barrier layer. Due to the symmetry-filtering effect, the TMR of epitaxial magnetic tunnel junctions can reach an order of magnitude above what is predicted by the Julliere or the Slonczewski models.

Lateral Symmetry of Bloch States in Electrodes

In the free-electron model for tunneling, the electrons are described as free electrons, with the only major difference from true free-electron states in terms of an effective mass not equal to the electron mass. When we use the free-electron model with an effective mass to approximate an actual Bloch state in a solid, we choose the effective mass such that the free-electron band dispersion is the same as the dispersion of the Bloch state. Although the effective mass theory has been used successfully for describing tunneling processes that do not involve the electron spin, it is inadequate for describing spin-dependent tunneling. We will show what is missing in the effective mass theory and why first-principles theory is needed for making predictions in magnetic tunnel junctions.

Symmetry of Bloch Wave Functions on a Square Lattice

If the Bloch state consists of mostly s (angular moment $l = 0$) atomic orbitals, which is the case for vast majority of semiconductors, then the free-electron wave function can also approximate the Bloch wave function. This explains why the effective mass model is so successful for semiconductors. In semiconductors the relevant electron bands to transport are mostly s-character. However, if the Bloch state is made up of p or d electrons, then the free-electron wave function can differ significantly from the actual Bloch electron wave function.

What affects the tunneling properties of electron states is the symmetry of the Bloch wave function within the plane perpendicular to the direction of transport. In this section we will examine this symmetry and the next section will show how the symmetry affects tunneling. We choose the coordinate system such that the plane is parallel to both the x and y directions. The wave function in the plane is simply $\psi(x, y)$. For the sake of discussion, let us also assume that this plane contains a lattice with square symmetry and a lattice constant a. If we denote the Bloch wave vector within the plane as (k_x, k_y), then the Bloch theorem for this two-dimensional wave function is

$$\psi_{k_x k_y}(x, y) = u_{k_x k_y}(x, y)\exp\left[i\left(k_x x + k_y y\right)\right], \tag{115}$$

and $u_{k_x}k_y$ is a periodic function. The free-electron effective mass model only takes into account the $\exp\left[i\left(k_x x + k_y y\right)\right]$ part of the wave function and treats $u_{k_x}k_y$ as a constant (Fig. 16).

In general, the periodic function $u_{k_x}k_y$ can be expanded in terms of plane waves on the two-dimensional reciprocal lattice $\mathbf{G}_n$,

$$u_{k_x k_y}(\mathbf{r}) = \sum_n a_n \exp(i\mathbf{G}_n \cdot \mathbf{r}). \tag{116}$$

Terms corresponding to different reciprocal lattice vectors have different symmetries. The origin of the reciprocal lattice, $\mathbf{G}_0 = 0$, gives a constant $u_{k_x}k_y$. This is the term that the free-electron effective mass model corresponds to.

The two different ways of describing the symmetry of the wave functions can be connected by evaluating the overlap integral between them. For example, the $\mathbf{G}_0 = 0$ wave function $\exp(i\mathbf{G}_0 \cdot \mathbf{r})$ is the same as the s orbital which is 1. So the cubic wave function with the lateral component described by $\mathbf{G}_0$ is predominantly s-character. Along the cubic (001) direction, this wave function is called the Δ_1 state. Within the two-dimensional plane, this wave function also has nonzero overlap integrals with the p_z and the $d_{2z^2-x^2-y^2}$ orbitals. So the Δ_1 state is mostly s-character but also contains some p_z and $d_{2z^2-x^2-y^2}$ components.

Similarly, the first reciprocal lattice vectors, $\mathbf{G}_1 = (\pm 2\pi/a, 0)$ and $(0, \pm 2\pi/a)$, give the antisymmetric plane-wave functions $\sin[(2\pi/a)x]$ and $\sin[(2\pi/a)y]$ and the symmetric $\cos[(2\pi/a)x]$ and $\cos[(2\pi/a)y]$. The antisymmetric pair has zero overlap integrals with the s orbital but have nonzero integrals with the p_x and p_y orbitals. These are called the Δ_5 states. The symmetric pair has zero integrals with all of the

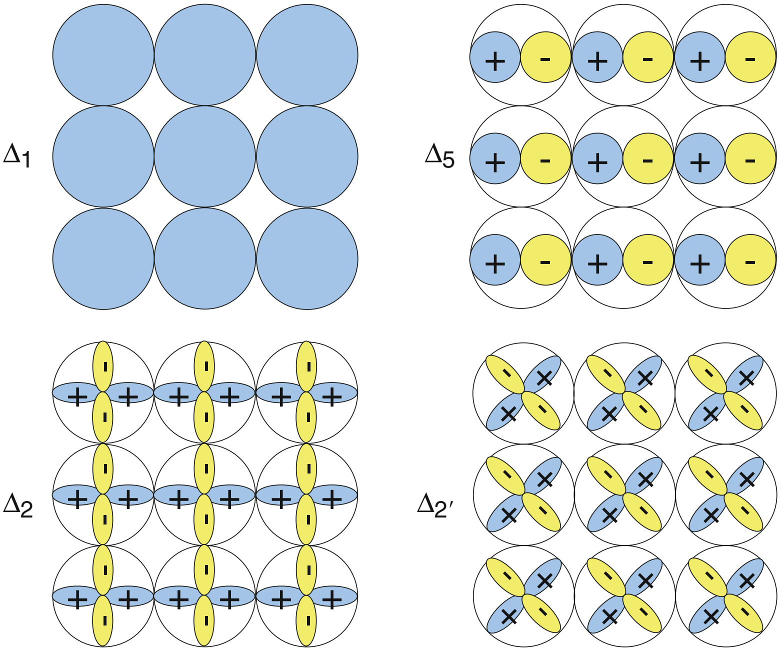

Fig. 16 Symmetry of wave functions of a two-dimensional square lattice

s and p orbitals, but has nonzero integrals with the $d_{x^2} - y^2$ orbitals. These are the Δ_2 states and are d character. Finally, one of the wave functions made from the second reciprocal lattice vectors, $\mathbf{G}_2 = (\pm 2\pi/a, \pm 2\pi/a)$, is $\sin[(2\pi/a)x] \sin[(2\pi/a)y]$. This is the $\Delta_{2'}$ state. It has no s or p component but has d_{xy} component.

Different Decay Rates of Bloch States in Barrier Layer

Although experimentalists like to fit the measured tunneling current to a simple free-electron model, such a model cannot correctly predict the spin dependence of the tunneling current. For example, in such a model there can be only a single decay rate for a given value of $k_{\|} = \sqrt{k_x^2 + k_y^2}$, and the tunneling current decays with the barrier thickness, d, as $\exp(-2kd)$ where $\kappa = \sqrt{\frac{2m}{\hbar^2}(V - E) + k_{\|}^2}$. Because this decay rate does not depend on the electron spin, the only possible spin dependence of the tunneling current must come from the spin polarization of the density of states in the electrodes. This prediction by the free-electron model does not agree with experiments. The spin polarization of the tunneling current can be determined experimentally by tunneling into superconductors. In the vast majority of the cases, the tunneling current has been found to be dominated by the majority spin electrons regardless of the spin polarization of the density of states, even in cases such as nickel and cobalt whose minority density of states is an order of magnitude larger than that of the majority. It turns out that the Bloch wave function symmetries in the electrodes can lead to different decay rates in the barrier layer. Consequently the barrier layer serves as a symmetry filter for tunneling electrons and only selectively passes through electrons with high symmetry. Because of the different wave function symmetries of the majority and minority electrons, symmetry filtering in the barrier layer becomes spin filtering. This in turn becomes the fundamental reason for very large tunneling magnetoresistance in epitaxial tunnel junctions based on MgO barriers.

The basic physical reason that the different Bloch states decay at different rates in the barrier is that they have different amounts of curvature in the plane parallel to the interfaces. We have shown in the previous section that these oscillations correspond to the two-dimensional reciprocal lattice vectors perpendicular to the direction of tunneling. Assume for simplicity that the boundary conditions at the edge of the barrier can be matched with the separable form $\psi(x,y,z) = \phi(x,y)\exp(-\kappa z)$. Then, for a wave function described by a two-dimensional reciprocal lattice vector, $\phi(x, y) = a_{\mathbf{G}} \exp[i(\mathbf{k}_{||} + \mathbf{G}) \cdot \mathbf{r}_{||}]$, the decay perpendicular to a simple barrier with potential V is given by

$$\kappa^2 = \frac{2m}{\hbar^2} V - |\mathbf{k}_{||} + \mathbf{G}|^2. \tag{117}$$

At each $\mathbf{k}_{||}$, there are as many different decay rates as are number of reciprocal lattice vectors. At normal incidence, $\mathbf{k}_{||} = 0$, the slowest decay rate corresponds to $\mathbf{G} = 0$ which for the square lattice is the Δ_1 state. The larger the value of $|\mathbf{G}|$, the faster the decay rate. Because of the connection between the reciprocal lattice vector in the plane-wave expansion and the s, p, d waves in the spherical harmonic expansion, states that are primarily s-like which have little curvature decay the slowest. p-like states will decay faster, and d-derived states, in particular, will be disadvantaged in penetrating the barrier because of their higher curvature due to additional nodes in the plane parallel to the barrier, requiring a plane-wave expansion that contains primarily $\mathbf{G}_2$.

The notion of multiple decay rates in a spatially homogeneous barrier layer may seem counterintuitive. To illustrate this more vividly, let us look at how electron wave functions at the Fermi energy of Fe(001) decay through a vacuum barrier. For this purpose, we calculate the modular square of the tunneling wave function with the boundary conditions that correspond to a unit flux of incident electrons in a single Bloch state on one side (left side in this case). For this calculation we choose the barrier height relative to the Fermi energy to be approximately equal to the work function in order to be an approximate representation of tunneling through vacuum. The results displayed in Fig. 17 show three decay rates. The majority Δ_1 state (which has s, p, d character) decays as $\kappa = \sqrt{\frac{2m}{\hbar^2}(V-E)}$, exactly as expected for the simple barrier model. The other states, however, decay more rapidly. The minority Δ_2 ($d_{x^2} - y^2$ symmetry) and all of the Δ_5 states (p_x and p_y) symmetry decay as $\kappa = \sqrt{\frac{2m}{\hbar^2}(V-E) + G_1^2}$ where $G_1 = 2\pi/a$. The majority and minority $\Delta_{2'}$

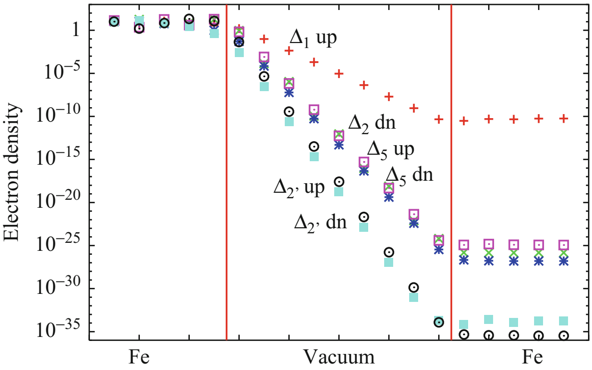

Fig. 17 Electron density for tunneling states at $k_{\|} = 0$ for Fe(001)/vacuum/Fe(001). Vacuum is approximated here by a spatially homogeneous barrier

states that have d_{xy} symmetry decay as $\kappa = \sqrt{\frac{2m}{\hbar^2}(V-E) + G_2^2}$ with $G_2 = \sqrt{2}2\pi/a$. G_1 and G_2 are simply the magnitudes of the first two reciprocal lattice vectors of the two-dimensional lattice parallel to the interfaces.

The lateral symmetry of the Δ_2 band and the Δ_5 band relates to the same reciprocal lattice vector G_2. For tunneling through vacuum these two states also see the same barrier height. Therefore, both states decay with the same rate in vacuum. However, an insulating material such as MgO does not map to a simple step barrier. As we will see next, the decay rates of electron wave functions in a barrier layer are determined by the so-called complex band structure. The complex bands in MgO for the Δ_2 symmetry and for the Δ_5 symmetry are completely different. Thus, the decay rates of these two bands in MgO are also different.

Symmetry Filtering in the Barrier Layer

Complex Band Structure of MgO (001)

The bandgap in the insulator layer can be accurately described by a two-band model [23],

$$-\frac{1}{k^2} = \frac{\hbar^2}{2m^*(E_1 - E)} + \frac{\hbar^2}{2m^*(E - E_2)}. \tag{118}$$

The right-hand side of the equation is negative for $E_2 < E < E_1$, yielding an imaginary k whenever E is inside the bandgap. This equation accurately describes the dominant complex band of MgO along the (100) direction, as shown in Fig. 18.

The complex band structure of the barrier layer is directly related to the tunneling conductance of a tunnel junction. The imaginary part of the wave vector represents the rate of decay of the evanescent electron wave function inside the barrier. In general, if the band dispersion is isotropic in k space, the transmission

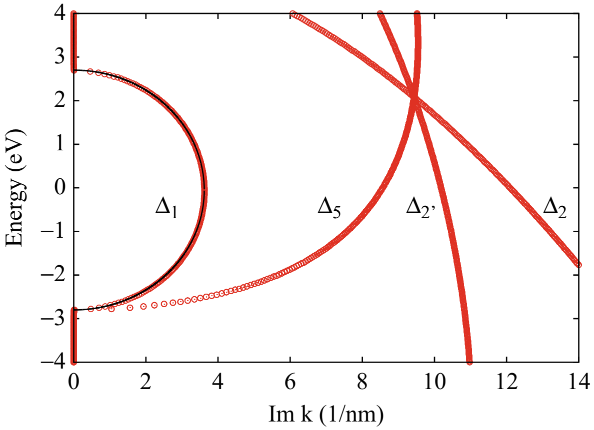

Fig. 18 The complex bands along the (100) direction of MgO. Data points are calculated with the layer-KKR code for an artificial MgO lattice constant of 2.03 Å which matches the bcc Fe lattice. The solid curve is the fit to the complex band with the smallest decaying wave vector using Eq. 118 with $m^* = 0.35$

contains a factor $\exp(-2kd)$ where d is the thickness of the barrier and k can be assumed to obey,

$$\kappa^2 = \kappa_0^2 + k_{\|}^2, \tag{119}$$

where $k_{\|}$ is the transverse wave vector (parallel to the interface) and $k_0 = ik$ is the imaginary part of the wave vector for normal incidence. Accounting only for the decaying of the wave function due to the complex wave vector, the conductance of a single k can be assumed to be approximately

$$G\left(k_{\|}\right) = \frac{2e^2}{h}\exp(-2\kappa d). \tag{120}$$

Such an assumption may not be very accurate in a real material. For now we assume that it is qualitatively correct and use it to calculate the conductance. The conductance is given by an integration over all $k_{\|}$,

$$G = \frac{2e^2}{h}\frac{1}{(2\pi)^2}\int_0^{\infty}\exp\left(-2\sqrt{\kappa_0^2 + k_{\|}^2}d\right)2\pi k_{\|}dk_{\|}. \tag{121}$$

Integrating and keeping only the leading term in $1/d$, we obtain

$$G = \frac{2e^2}{h}\frac{\kappa_0}{4\pi d}\exp(-2\kappa_0 d). \tag{122}$$

Thus, the product Gd scales with the barrier thickness as a simple exponential with an exponent of $2\kappa_0$. For thick barriers, the complex bands accurately predict the thickness dependence of the tunneling resistance.

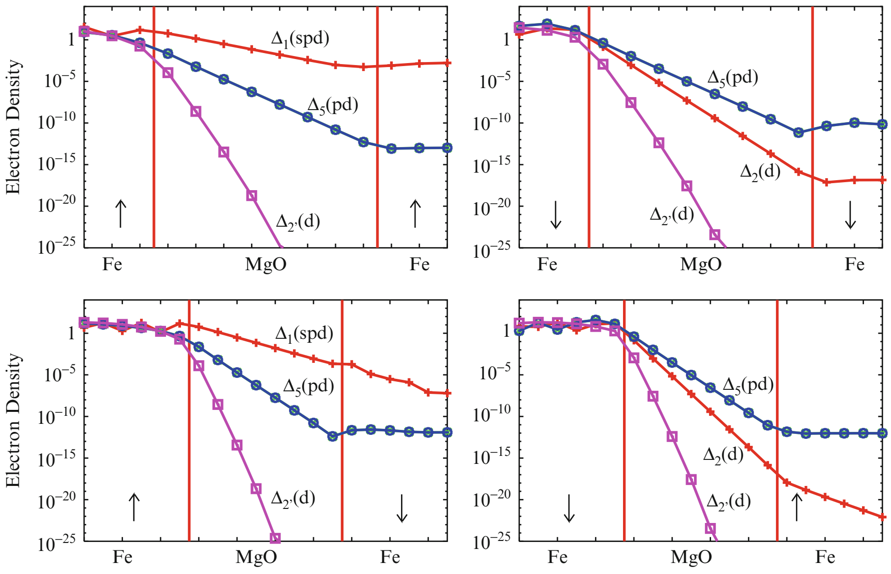

Fig. 19 Density of the tunneling electron states at $\mathbf{k}_{\parallel} = 0$ for Fe(001)|8MgO|Fe(001). The four panels show the states for majority (*upper left*), minority (*upper right*), and antiparallel alignment of the moments in the two electrodes (*lower panels*). Additional Fe layers are included in the *lower panels* to show the electron density variation for the tunneling states extending into the *right* Fe electrode. Each *curve* is labeled by the symmetry of the incident Bloch state in the *left* Fe electrode

Symmetry Filtering in MgO Barrier Layer at Normal Incidence

Let us first examine how electrons are transmitted through a MgO barrier layer if they are incidentally perpendicular to the interface. Using the language of Bloch wave vectors, these are the electrons whose k_x and k_y, the two components parallel to the interface, are exactly zero. The decay rates of the electron wave functions are determined by the complex band structure we just discussed. Because of the two-dimensional lattice periodicity, during tunneling the crystal momentum parallel to the layers $\mathbf{k}_{\parallel} = (k_x, k_y)$ is conserved except that it may be changed by a reciprocal lattice vector. Tunneling with the conservation of $\mathbf{k}_{\parallel}$ in this manner is called specular transmission. In Fig. 19, we show the density of tunneling states associated with each of the Fe(001) Bloch states having $k_{\parallel} = 0$ for an Fe/MgO/Fe tunnel junction, similar to the plot for the vacuum barrier, Fig. 17.

At $\mathbf{k}_{\parallel} = 0$, the lateral components of the wave functions in the electrodes from the different bands have distinct symmetries. Not only their symmetries have to match those inside the barrier layer, they must also match the symmetry on both sides in order for electrons to be transmitted. When such matching of the symmetry cannot be found on both electrodes, the transmission is zero even when the barrier layer admits such wave functions. Spin-dependent tunneling is thus achieved through selective filtering of wave functions with different lateral symmetries and by virtue of the fact that wave functions in the two spin channels do not have the same symmetries.

As an example, we show in Fig. 19 the density of tunneling electron states for an Fe/MgO/Fe junction. The top two panels show the plots when the moments of the two Fe electrons are aligned parallel. In this case, the majority spin channel (top left panel) has a Δ_1 state with a large transmission probability, providing a large tunneling current. The Δ_5 electrons decay faster in the MgO layer, leading to a smaller transmission. The $\Delta_{2'}$ electrons decay extremely fast within MgO and provide negligible tunneling current. The minority spin Fe (top right panel) does not have Δ_1 state, thus having a much reduced transmission. For the antiparallel moment alignment, the left-hand side of the lower left panel shows that the Δ_1 electrons of the majority bands readily enter the MgO where they decay slowly with distance as predicted by the corresponding complex band of MgO. Once these electrons exit the barrier and enter the right Fe electrode, however, because there are no Fe minority Δ_1 Bloch states at the Fermi energy, they continue to decay within the right Fe electrode leading to zero transmission. On the other hand, although the Δ_5 electrons decay relatively rapidly in the MgO, because there are minority spin Δ_5 states in the right electrode, these electrons have a finite transmission. Similarly, in the lower right panel of Fig. 19, the minority Δ_2 state decays as a $\Delta_{2'}$ state within the MgO and continues to decay within the majority Fe layer because there is no Δ_2 state at the Fermi energy in majority Fe. Again, the Δ_5 electrons decay rapidly but can enter the minority Fe while the minority Fe $\Delta_{2'}$ electrons decay extremely rapidly. In this manner, a large difference in the transmission between the parallel and the antiparallel spin configurations is established.

Because of the complete reflection of the Δ_1 electrons at $k_{||} = 0$, the maximum conductance for antiparallel alignment does not occur exactly at $k_{||} = 0$.

The "missing" of the Δ_1 band within a certain energy range in the (100) direction of the bcc metal is a common feature due to the hybridization of the "*s*-band" with the *d*-bands. In the band structure of a typical bcc transition metal, the *s*-band starts from the Γ point a few eV below the *d*-bands. Its energy rises rapidly with $\mathbf{k}$ until it reaches the energy range of the *d*-bands. Near the bottom of this energy range, the *s*-band hybridizes heavily with the *d*-bands, causing it to flatten out and end at the Brillouin zone boundary. The part of the *s*-band above the energy range of the *d*-bands can also be followed downward in energy. It is again highly dispersive until it approaches the top of the energy range for the *d*-bands at which point it flattens out and intersects the zone center at the $\Gamma_{2'}$ point. In the (001) direction, the "*s*-band" has the Δ_1 symmetry, and there is a range of energy over which there is no Δ_1 band. For bcc iron, the spin splitting is such that the majority Δ_1 band crosses the Fermi energy, but there is no minority Δ_1 band near the Fermi energy, while there are *d*-bands crossing the Fermi energy in both spin channels.

Ballistic Tunneling in Fe/MgO/Fe

The Landauer formula, Eq. 106, relates the conductance of a tunnel junction to the sum of the transmission probabilities of the electron wave function over all values of $\mathbf{k}_{||}$. Although the total transmission determines the tunneling conductance and the magnetoresistance, the dependence of the transmission on $\mathbf{k}_{||}$ can also reveal interesting physics about the spin-dependent tunneling process. In some cases, such $\mathbf{k}_{||}$ dependence can manifest itself as unexpected barrier thickness dependence, as we will see in this section in the cases of interference of tunneling states and transmission through interface resonance states.

Majority Spin Transmission: Interference of Tunneling States

We begin our discussion by presenting the first-principles calculation with the layer Korringa-Kohn-Rostoker (layer-KKR) method [16]. In this calculation the electrode layers of Fe are fixed at the experimental lattice constant of 2.866 Å, and the in-plane MgO lattice constant (along the [100] axis) is $\sqrt{2}$ times larger or 4.053 Å. The out-of-plane MgO lattice spacing (along [001]) is fixed at 2.21 Å, the experimental value [24]. The calculated transmission probability as a function of $\mathbf{k}_{||} = (k_x, k_y)$ for the majority spin channel, when the moment in both Fe electrodes is aligned parallel to each other, is shown in Fig. 20 for 4, 8, and 12 layers of MgO. The transmission has a peak centered at $k_{||} = 0$. Comparing the three panels of Fig. 20, we see clearly the increasing concentration of the transmission in the region near $k_{||} = 0$ as the insulating barrier layer is made thicker. This general feature is expected from a barrier for which the transmission probability contains a factor exp $(-\kappa d)$ where κ approximately follows Eq. 119. However, the detail of the dependence of the transmission on $\mathbf{k}_{||}$ is much more complex and deviates significantly from Eq. 119, as is shown in Fig. 21 which plots the transmission probability as a function of k_x for $k_y = 0$ and compares it against Eq. 119.

The most striking feature in Fig. 21 is that the k_x dependence of the transmission probability is oscillatory, indicating that there is wave interference within the barrier. This oscillation is the result of the interference of two tunneling states within the barrier layer, a phenomenon that occurs in a crystalline barrier but not in vacuum or an amorphous barrier. This phenomenon was predicted and analyzed theoretically [23] and later was used to explain the oscillatory dependence of the magnetoresistance on the barrier layer thickness [25].

For interference to occur within the barrier layer, there has to be at least two different complex bands at the same value of $k_{||}$, and these bands must also decay at exactly the same rate in the barrier. This indeed is the situation for certain values of $k_{||}$ away from the normal incidence. The complex values of k_z at the Fermi energy are plotted as a function of $k_{||}$ in Fig. 22. The two states shown have the lowest value of the imaginary part of k_z and are therefore the most important for determining the

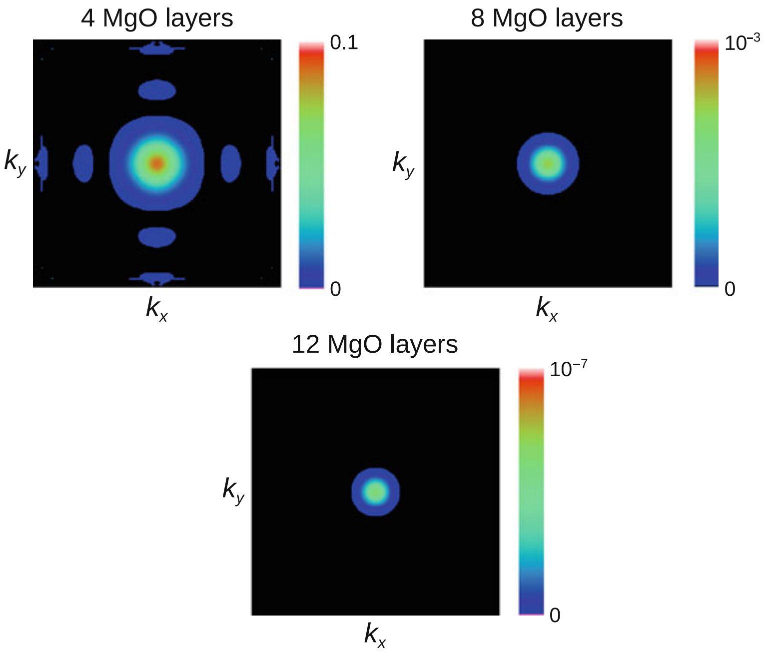

Fig. 20 Majority spin transmission probability for 4, 8, and 12 layers of MgO and parallel alignment of the moments in the Fe electrodes. Units for k_x and k_y are inverse Bohr radii

Fig. 21 Majority transmission probability as a function of k_x for $k_y = 0$ for 4 and 8 layers of MgO. The curves end before the zone boundary is reached because there are no states for $k_x > 0.55(\text{a.u.})^{-1}$. *Dotted red curves show the expected behavior of the transmission probability from Eq.* 119

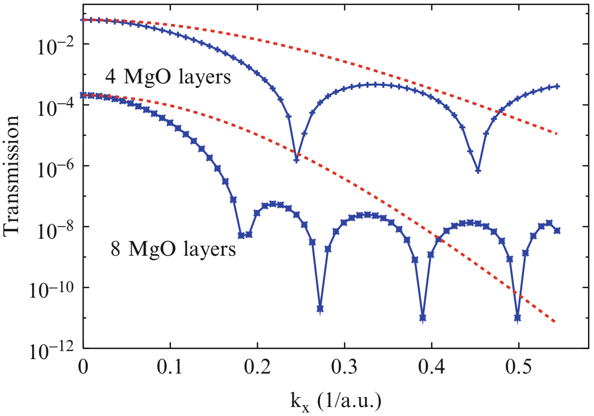

transmission probability. The states are plotted as a function of $k_{\|}$ along $\overline{\Gamma}$ to $\overline{X}$. At $k_x = 0$, the two states shown are the Δ_1 and one of the Δ_5 states. As k_x increases from zero, their real part increases linearly from zero and is the same for both states. At $k_x \Delta z \approx 0.59$, the imaginary parts of the two states become equal and the real parts bifurcate. Afterward, the imaginary part remains approximately constant.

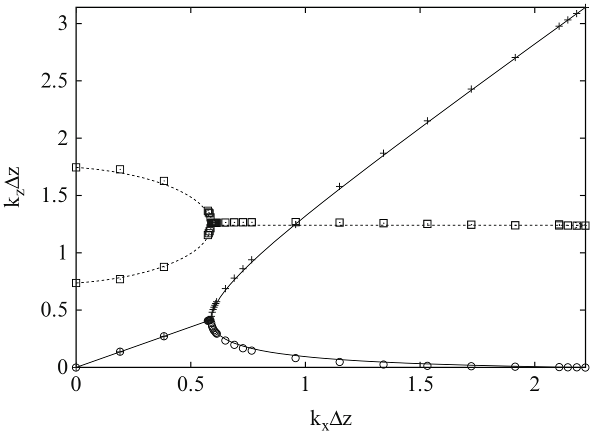

Fig. 22 Real and imaginary parts of k_z plotted as a function of k_x for MgO. The two values of k_z with the smallest imaginary parts are shown. *Circles* (*squares*) denote values of the real (imaginary) part of k_z calculated with the layer-KKR code. The *solid line* and *dotted lines* are the real and imaginary parts, respectively, of the fit to complex k_z described in the text

The real parts of $k_z\Delta z$ for the two states reach n and 0, respectively, at the zone boundary which occurs at $k_x\Delta z = \pi/\sqrt{2}$.

We focus on the part of Fig. 22 where the two states have the same imaginary part of $\mathrm{k_z}$. This is the region between $k_x\Delta_z = 0.59$ and the zone boundary. Suppose that a wave function is a linear combination of two decaying waves with the two complex wave vectors depicted in this region,

$$\psi(z) = Ae^{ik_1 z} + Be^{ik_2 z}, \tag{123}$$

then the electron density exiting the barrier is given by

$$|\psi(d)|^2 = e^{-2\kappa(k_x)d}\left\{|A|^2+|B|^2 + 2\mathrm{Re}(A^*B)\cos\left[k_1^r(k_x)d - k_2^r(k_x)d + \phi\right]\right\} \tag{124}$$

where k_1^r and k_2^r are the real parts of the two values of k_z, κ is their common imaginary part, and ϕ is the relative phase between the complex coefficients A and B. Thus, the transmission is a damped oscillatory function of thickness and is a purely oscillatory function of k_x since κ is essentially independent of k_x for $\mathrm{k_x}\Delta z > 0.59$.

The interference between different tunneling states is a general phenomenon. For any barrier material, the dispersion relation in the vicinity of the gap can be expressed as a polynomial in $\cos k_z \Delta z$ with real coefficients that depend on k_x and k_y,

$$E_{\mathbf{k}} = \sum_n A_n\left(k_x, k_y\right)\ \left(\cos k_z\Delta z\right)^n. \tag{125}$$

Inside the bandgap, all solutions of k_z for a given real $E_{\mathbf{k}}$ are complex and must be in pairs, i.e., both k_z and its complex conjugate are roots of Eq. 125. Now consider the pair of roots with the smallest imaginary part, $r = \cos k_z \Delta z$ and $r^* = \cos k_z^* \Delta z$.

Defining $s = e^{ik_z\Delta z}$ so that $\cos k_z\Delta z = (s + s^{-1})/2$, the values of $k_z\Delta z$ can be found from the equations,

$$s^2 - 2rs + 1 = 0 \tag{126}$$

and

$$s^2 - 2r^*s + 1 = 0. \tag{127}$$

Each of these equations has two roots, $s_1^\pm = r \pm \sqrt{r^2 - 1}$, $s_2^\pm = r^* \pm \sqrt{(r^*)^2 - 1}$. Because $s_1^+ s_1^- = s_2^+ s_2^- = 1$, we know that only two of these roots will represent decaying waves. Thus, if $|s_1^+| < 1$, it follows that the two decaying roots, s_1^+ and s_2^+, have equal modulus,

$$e^{-\mathrm{Im}k_{1z}\Delta z} = |s_1^+| = |s_2^+| = e^{-\mathrm{Im}k_{2z}\Delta z}. \tag{128}$$

Thus, the imaginary parts of $k_z\Delta z$ for these two solutions are equal. This would lead to the observed interference effect.

In order for the interference effect to be observable experimentally as an oscillation of the tunneling magnetoresistance, it is necessary that the decay rate of the tunneling states that produce the interference effect to be the same as that of the dominating tunneling state, which in the case of Fe/MgO/Fe is the Δ_1 state. This seems unlikely because all other states decay faster than the Δ_1 state in ballistic tunneling. It turns out that the effect of nonspecular (diffusive) tunneling produces a scatter-in term which makes all states decay at the same rate within the barrier layer [25]. Thus, the interference of the tunneling states can indeed be observed as an oscillation of the tunneling conductance and TMR as a function of the barrier layer thickness [24, 26].

Minority Spin Transmission: Tunneling Through Interface Resonance States

The transmission probability for the minority spin channel for the parallel moment alignment is shown in Fig. 23 for three different MgO layer thicknesses. The dependence on $\mathbf{k}_{||}$ for the minority spin transmission is dramatically different than for the majority spin. The minority spin transmission has a complicated, sharply peaked structure with peaks away from $\mathbf{k}_{||} = 0$. These peaks do not correspond to anything in the bulk Fe electronic structure. Instead, they arise from resonant states localized on the Fe/MgO interface.

The interface resonant states are similar to surface states in that both are electron energy eigenstates localized at the boundaries of the material. The eigenstates of an electron in a perfect crystal are the Bloch states which satisfy the Bloch periodic boundary conditions. These states are described by a wave vector $\mathbf{k}$ which has to

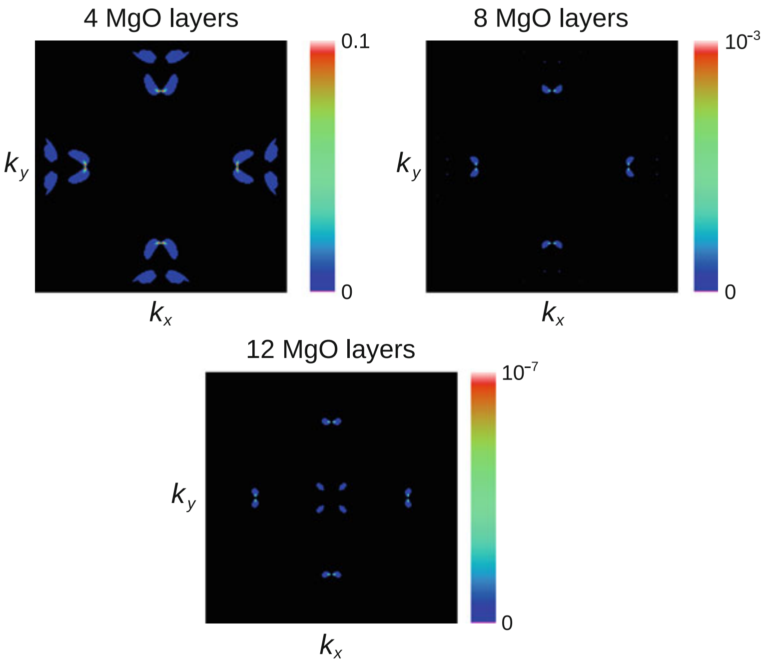

Fig. 23 Minority transmission probability for 4, 8, and 12 layers of MgO and parallel alignment of the moments in the Fe electrodes. Units for k_x and k_y are inverse Bohr radii

be real. Although there are also evanescent states that satisfy the Schrodinger equation for a perfect crystal, these states are not physically acceptable solutions because they diverge to infinity along one direction. At a surface or an interface, however, the periodicity of the lattice is interrupted, and the evanescent states become valid solutions for the material. These are the surface or interface states. True surface states are orthogonal to the bulk Bloch states. There are also surface or interface states that are coupled to the bulk Bloch states. These states are usually called resonance states. Interface resonance states in a magnetic tunnel junction can have a large impact on spin-dependent tunneling.

In general, the interface resonance states are needed to properly match the boundary conditions for the electron wave functions across an interface. This is because at a fixed energy, the Bloch states alone do not form a complete basis. The collection of all Bloch states and evanescent waves (traveling or decaying) along a single direction forms a 2D complete basis set. However, the boundary conditions for an incident wave function include both the values of the wave function on a plane and its normal derivative. To satisfy both boundary conditions, there needs to be two independent complete basis sets. For example, consider a transmission problem with a single Bloch wave function of the left electrode incident on a tunnel barrier. In order to properly match the boundary conditions, we must use all the evanescent waves inside the barrier, plus all of the left-traveling Bloch states (i.e., reflected waves) and the evanescent waves on the electrode side, the latter decaying into the electrode. Under certain conditions, these evanescent waves form the interface resonance states. Written out explicitly, the boundary conditions are matched as

$$\psi^L_{k_z,\mathbf{k}_{||}+\mathbf{G}} + r\psi^L_{-k_z,\mathbf{k}_{||}+\mathbf{G}} + \sum_{\mathbf{G}'} r_{\mathbf{G}\mathbf{G}'}\psi^L_{\mathbf{k}_{||}+\mathbf{G}'} = \sum_{\mathbf{G}'} t_{\mathbf{G}\mathbf{G}'}\psi^B_{\mathbf{k}_{||}+\mathbf{G}'}, \qquad (129)$$

where the three terms on the left-hand side are the incident wave, principal reflected wave, and additional reflected wave components which include evanescent waves in the left electrode, respectively. On the right-hand side we include only the decaying evanescent waves into the barrier and omitted the growing evanescent waves. For sufficiently thick barriers, the growing evanescent states into the barrier can be neglected. The evanescent waves in the third term on the left-hand side are the interface resonance states.

When the first two terms on the left-hand side of Eq. 129 have the same symmetry as the leading evanescent wave on the right-hand side, the contribution from other evanescent waves is small, and the transmission is essentially determined by the evanescent wave with the same symmetry as the incident wave. This is usually the case for the majority spin channel. But when the dominating evanescent wave function in the barrier layer matches poorly to the incident Bloch wave, the third term in Eq. 129 becomes important. Which evanescent term on the electrode side is the largest is determined entirely by the boundary conditions. For some values of $\mathbf{k}_{||}$, the largest evanescent term has a very large decaying wave vector. As a result, the total wave function rises as a fast exponential toward the interface. Because of the exponential nature of these evanescent states, any small change in the boundary conditions can cause large changes in the total wave function, making it a sensitive function of $\mathbf{k}_{||}$. Consequently the transmission plotted in the reciprocal space appears to have very sharp peaks as characteristics of interface resonance states.

The interfacial resonance state is important to the transmission because it yields a huge wave function amplitude at the interface. However, it is only part of the story. For example, in Fe/MgO/Fe the minority spin channel electron state density as a function of $\mathbf{k}_{||}$ usually peaks at points along symmetry axes where the interface resonance is the strongest. But the transmission is quite low at these points. The second major factor determining the transmission is the wave function symmetry. This is because the Bloch states along these symmetry axes have no s-character. They can only couple to evanescent states in the MgO that decays rapidly. Very slightly away from these symmetry axes, the wave function has significant s-character and can couple to an evanescent state that decays slowly. Therefore, the strongest transmission due to interface resonances usually occurs close to but slightly off the symmetry axes, as shown in Fig. 23.

The transmission as a function of $k_{|}|$ for antiparallel alignment of the moments (Fig. 24) shows a combination of the features observed in the majority and minority channels. For thinner layers, the highest transmission is near the line $k_y = 0$ in the

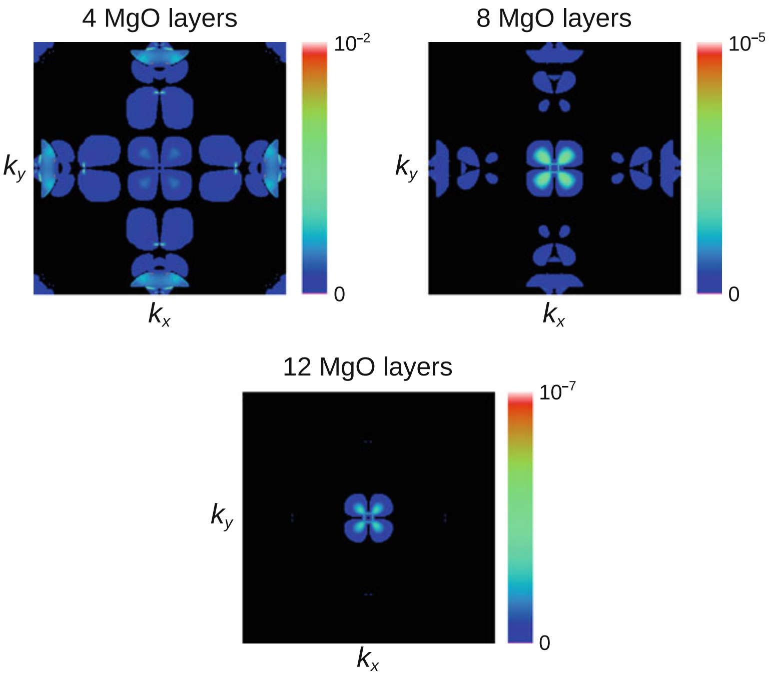

Fig. 24 Transmission probability for antiparallel alignment of the moments in the Fe electrodes

two-dimensional zone where there is an interfacial resonance state. As the layers become thicker, the highest transmission occurs closer to the origin of the two-dimensional zone.

Thickness Dependence of the Tunneling Conductance

Although the dominant factor in the thickness dependence of the tunneling conductance is the exponential factor $\exp(-\kappa d)$ where κ is the imaginary part of the complex band wave vector and d is the thickness of the barrier layer, the actual thickness dependence is not simply an exponential function. The same simple model, Eq. 119, of an isotropic complex band at the $\overline{\Gamma}$ point gives the conductance for each spin channel in the form

$$G = \gamma A \frac{e^2}{h} \frac{1}{(2\pi)^2} \int_0^\infty \exp\left(-2\sqrt{k_\parallel^2 + \kappa_0^2 d}\right) 2\pi k_\parallel dk_\parallel. \tag{130}$$

This equation works directly for the majority spin channel in R_P. Neglecting the contribution from the minority spin channel, we find

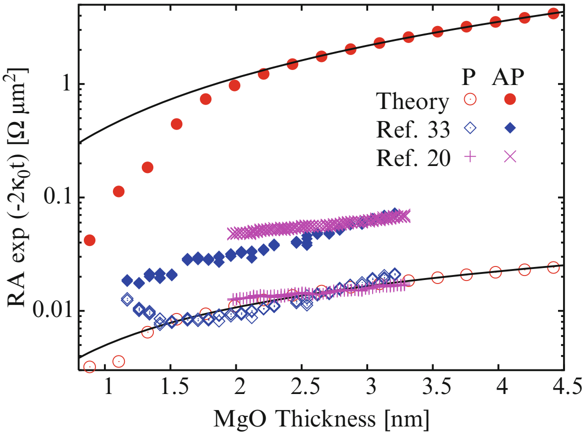

Fig. 25 Sheet resistance of an Fe/MgO/Fe tunnel junction as a function of MgO thickness t, scaled by $\exp(-2\kappa_0 t)$. Layer-KKR calculation (*open circle*, R_P; *filled circle*, R_{AP}) is compared to two experiments (*open diamond*, R_P from Ref. [24]; *filled diamond*, R_{AP} from Ref. [24]; *plus*, R_P from Ref. [26]; *cross*, R_{AP} from Ref. [26]). The *solid curves* are fits to layer-KKR results using Eqs. 131 and 133

$$R_P A = \frac{8\pi h}{\gamma_P e^2} \frac{\exp(2\kappa_0 d)}{\dfrac{1}{d^2} + \dfrac{2\kappa_0}{d}}. \tag{131}$$

Using γ_P as the only fitting parameter, this result fits the layer-KKR calculation of R_P very well, as shown in Fig. 25, except for the first two points where the minority spin channel still contributes significantly to the total conductance. In order to make this comparison more clearly, we first calculated the complex band structure at the Fermi energy of the Fe electrodes for a bulk MgO lattice built using the self-consistent potential of the middle MgO layer of an Fe/6MgO/Fe tunnel junction. The complex band calculation yields $\kappa_0 = 2.92\ \text{nm}^{-1}$ for the Δ_1 band at $\mathbf{k}_{||} = 0$. This number is used as the baseline decay rate of the tunnel wave functions: the baseline exponential factor $\exp(2\kappa_0 d)$ was removed from the calculated total tunneling conductance of the Fe/MgO/Fe tunnel junction as a function of the MgO thickness, resulting in the plot of Fig. 25.

For the AP configuration, the Δ_1 band at $\overline{\Gamma}$ point cannot enter the opposite electrode. We modify the contribution to the conductance from $\mathbf{k}_{||}$ by multiplying a factor $1 - \exp\left(-\alpha k_{||}^2\right)$, which suppresses the conductance at $k_{||} = 0$, to mimic the effect,

$$G_{AP} = \gamma_{AP} A \frac{e^2}{h} \frac{1}{(2\pi)^2} \int_0^\infty \exp\left(-2\sqrt{k_{||}^2 + \kappa_0^2}\, d\right) \left[1 - \exp\left(-\alpha k_{||}^2\right)\right] 2\pi k_{||} dk_{||}. \tag{132}$$

Integrating and assuming that $\alpha\kappa_0^2 \gg 1$, we find

$$R_{AP} A = \frac{4\pi h}{\gamma_{AP} e^2} \frac{d^2 + \alpha\kappa_0 d}{\alpha\kappa_0^2} \exp(2\kappa_0 d). \tag{133}$$

The two parameters γ_{AP} and a are treated as fitting parameters when we compare this formula to the layer-KKR calculation in Fig. 25. The agreement for R_{AP} is very well for large MgO thicknesses. At small thicknesses, the disagreement comes from the interface resonance states which contribute significantly to the AP conductance for thin MgO barriers.

The layer-KKR results are also compared to two experiments in Fig. 25. The agreement for R_P is surprisingly good, especially considering that there are no adjustable parameters in the calculation. This agreement demonstrates two points. First, the nonspecular scattering seems to have little effect on R_P. Second, the local density approximation (LDA) produces decay wave vectors at the Fermi energy that are in excellent agreement with experiments. In other words, the bandgap error in the LDA does not seem to affect the calculated tunneling current in the linear response regime. The significantly larger resistance in experimental measured samples for MgO thickness smaller than 1.5 nm is due to increased diffusive scattering rates in these samples. On the other hand, the experiments disagree with the calculated R_{AP} by more than an order of magnitude. This difference arises from diffusive scattering from defects inside the barrier and is not included in the calculation.

Other Epitaxial Tunnel Junctions

The principle of spin-dependent tunneling by symmetry filtering within the barrier layer is quite general for epitaxial tunnel junctions. Half-metallic ferromagnetic electrodes (i.e., ferromagnets with states of only one spin channel at the Fermi energy) are not required in order to obtain very large TMR. If one can achieve sufficiently good two-dimensional periodicity within the barrier and near the interface that $k_{||}$ is reasonably well conserved, i.e., the scattering is mostly specular, then one may take advantage of a class of electrode-barrier combinations in which some of the states of one spin channel decay much more slowly in the barrier than those of the other. There have been some works to explore different electrode materials and barrier materials that can be used to achieve symmetry filtering. For electrode materials, the requirements are that they must be ferromagnetic and that they must be able to form epitaxial junctions with an insulator or a semiconductor. Simple ferromagnetic materials include Fe, Co, and Ni. There are more complex magnetic materials such as Heusler alloys which have also been studied.

Co(bcc)/MgO/Co(bcc) and FeCo/MgO/FeCo

Because it is much easier to find matching 2D lattices with the square symmetry between a metal and an oxide, the best candidates for ferromagnetic electrodes are ones with a cubic lattice. Iron is bcc at room temperature and below. Although the bulk ground state for cobalt is hcp, thin cobalt bcc films can be grown epitaxially,

Table 2 Tunneling conductivity (in $1/\Omega m^2$) for all spin channels for the Co(bcc)/MgO/Co(bcc), FeCo/MgO/FeCo, and Fe/MgO/Fe tunnel junctions. Each junction contains eight atomic layers of MgO. Resonant state contributions to the minority spin channel are excluded

Junction material	↑↑	↓↓	↑↓(↓↑)	σ_P/σ_{AP}
FeCo/MgO/FeCo	1.19×10^9	2.55×10^6	1.74×10^6	340.5
Co/MgO/Co	8.62×10^8	7.51×10^7	3.60×10^6	130.2
Fe/MgO/Fe	2.55×10^9	7.08×10^7	2.41×10^7	54.3

and Co(bcc)/MgO/Co(bcc) magnetic tunnel junctions can also be made. Compared to Fe/MgO/Fe junctions, cobalt junctions have certain advantages. First, cobalt is less easy to oxidize than iron, so it is less likely to form an oxide layer on the interface with MgO which can greatly diminish the spin-filtering effect. The second advantage is that in bcc cobalt along the (100) direction, the majority bands and minority bands are completely orthogonal to each other at the Fermi energy. In order words, there are no common bands shared by the majority and minority spins. This helps to enhance the spin-filtering effect in Co/MgO/Co junctions and can potentially lead to higher TMR than in Fe/MgO/Fe.

The FeCo alloy combines the advantages of both iron and cobalt. On the one hand, FeCo alloy has nearly as good selectivity as cobalt in terms of spin filtering. On the other hand, FeCo has the ground state of B2 structure which is equivalent to the bcc lattice of a pure material. Therefore, in practice it is much easier to grow FeCo/MgO/FeCo junctions than Co(bcc)/MgO/Co(bcc) junctions. As we show below, the FeCo electrodes also lead to higher TMR. Most of magnetic tunnel junctions in use are based on FeCo electrodes (except for a small amount of boron which makes the as-deposited electrode amorphous to improve the formation of crystalline MgO during annealing).

The tunneling conductance for the three types of electrodes, bcc Fe(001), bcc Co(001), and B2 FeCo(001), all using an eight atomic layer MgO(001) barrier, is shown in Table 2. These calculations are done by integrating the transmission probability over the entire two-dimensional Brillouin zone with 8256 $\mathbf{k}_{||}$ points in 1/8th of the zone. For the minority spin channel, interfacial resonance states generate extremely sharp peaks as a function of $\mathbf{k}_{||}$. The contributions from these peaks are omitted because they are difficult to calculate accurately and are usually absent under experimental conditions. These contributions would have made the calculated TMR higher for the Co and FeCo electrodes because they contribute to the minority spin conductance for parallel moment alignment but do not contribute significantly to the antiparallel conductance. On the other hand, for Fe/MgO/Fe the interface resonance states contribute to both the parallel minority conductance and the antiparallel conductance and would lead to a reduced TMR.

From Table 2 we can see that both Co/MgO/Co and FeCo/MgO/FeCo have even larger TMR than Fe/MgO/Fe. The main reason for the larger TMR is that because in

Co/MgO/Co and FeCo/MgO/FeCo there are no Bloch eigenstates in the minority spin channel with Δ_1 symmetry in both materials, for the antiparallel spin alignment, all states are completely reflected at $\mathbf{k}_{||} = 0$. For bcc cobalt and bcc FeCo, no minority Δ_1 band crosses the Fermi energy, and the only band that crosses the majority Fermi energy is a Δ_1 band. This contrasts sharply with bcc iron for which in addition to the Δ_1 band, there are other bands in the majority channel that cross the Fermi energy at $\mathbf{k}_{||} = 0$. These additional bands have the same symmetry as those in the minority channel, which allow the transmission through the barrier.

The presence of some types of disorder may not greatly diminish the strong spin filtering in tunnel junctions made of cobalt and FeCo electrodes. For strongly magnetic alloys, i.e., those with filled majority *d*-bands, the moments are such that the bands match extremely well in the majority channel. Therefore, $k_{||}$ conservation arguments can be applied to majority electrons. The problem will be in the minority channel where the scattering is expected to be relatively strong. Even there, however, the bcc Co and FeCo electrodes should offer the possibility for relatively large TMR. Consider the case of antiparallel alignment. Majority electrons injected from the left electrode will decay slowly in the MgO barrier. When they encounter the right electrode, however, the (initially) Δ_1 states that would decay exponentially if the electrode were well ordered will continue do so for several layers until diffuse scattering converts a significant fraction of the surviving flux into symmetries that can propagate.

Experimentally, CoFe electrode was among the first electrodes used in magnetic tunnel junctions. Unlike pure Fe electrode which usually needs to be grown through MBE in order to ensure high-quality junctions, CoFe electrode can be grown using the much cheaper sputtering method and can form good epitaxial junctions through appropriate annealing. In addition, CoFe is less likely than pure Fe to oxidize and form the FeO interface layer that often greatly diminishes the TMR. Parkin et al. [27] made sputtered CoFe/MgO/CoFe junctions on an amorphous substrate that reached 220 % TMR at room temperature.

Today the standard technique to grow CoFe/MgO/CoFe junctions is to start from amorphous CoFeB. First a sandwich structure of CoFeB/MgO/CoFeB is deposited. Then through annealing, (100) textured CoFe/MgO/CoFe junction is formed. The advantage of starting from amorphous CoFeB is that it allows the junction to grow easily on top of synthetic antiferromagnetic substrates [28]. Also because of its amorphous lattice structure, CoFeB has a smaller strain with MgO than crystalline CoFe. This reduces interface roughness and facilitates the growth of MgO(100). During annealing, MgO(100) acts as a template for the crystallization of bcc CoFe on both sides of the barrier layer [29]. The boron atoms diffuse very fast during annealing and are generally believed to diffuse away leaving a clean CoFe/MgO interface. There is also evidence that some of the boron atoms may diffuse into the barrier layer [30, 31]. This could have an impact on the structure and electronic properties of the barrier layer, which will be discussed later.

Effect of Interlayers

Inserting interlayers between the electrodes and the barrier layer is a convenient way to modify the properties of magnetic tunnel junctions. One motivation of adding interlayers in particular is to prevent the formation of FeO on the interfaces which is shown to be very harmful to high TMR. Naturally the inserted interlayer would serve to separate the iron atoms from the oxygen atoms in the barrier layer. Two of the popular choices for interlayer materials are cobalt and magnesium. Other choices include silver and chromium. A common requirement for these interlayers is that they do not alter the two-dimensional square symmetry of the electrodes and the barrier layer.

Cobalt Interlayer

Because Co/MgO/Co and CoFe/MgO/CoFe junctions both have very large TMR, cobalt is a natural choice for interlayers in Fe/MgO/Fe or CoFe/MgO/CoFe. First of all, the electronic structure of the inserted cobalt layer is sufficiently close to that of the iron or CoFe electrodes, in which it is not expected to negatively impact spin filtering due to band symmetry. In addition, cobalt moments are more "robust" in the sense that it is less likely to have "loose spins" on the interface due to roughness than iron atoms. Furthermore, cobalt is more resistance to oxidization than iron. In fact, even in the experiment nominally examining Co(bcc)/MgO/Co(bcc), the thickness of the cobalt electrode layers is only four atomic layers thick [32, 33] in order to retain the bcc structure. Therefore, such a structure is better described as an Fe/Co/MgO/Co/Fe system containing cobalt interlayers.

Ideal epitaxial cobalt interlayer is predicted by first-principles calculation to cause a number of effects [34]. The first effect of adding cobalt interlayers is that it suppresses the interface resonance states due to the iron *d*-bands. This could boost TMR if these interface resonance states contribute more conductance to the AP spin configuration than to the P configuration. As more cobalt layers are added, the quantum well states confined within the cobalt layers move across the Fermi energy one by one, causing the tunneling conductance and TMR to oscillate with the number of atomic cobalt layers. As far as the TMR is concerned, a single atomic layer of cobalt seems to be the optimal thickness. A similar effect was also predicted with a single atomic layer of silver interlayer [35]. For thicker cobalt interlayers, interface resonances that correspond to cobalt d-bands start to appear. These interface resonances tend to increase the minority spin and antiparallel tunneling conductances, and consequently TMR decreases somewhat.

Magnesium Interlayer

Another special interlayer material is magnesium. An ultrathin magnesium layer is often deposited on the iron electrode before depositing the MgO layer in order to prevent the oxidization of the iron electrode which can greatly diminish the TMR. In addition, the magnesium layer may also serve as a crystalline seed to improve the texture of the MgO layer and the interface structure. Because magnesium does not have an intrinsic spin polarization, the concern is whether adding the magnesium layer would reduce the TMR by reducing the spin polarization of the incoming current. Experiments show that inserting one or two atomic layers of magnesium have a moderate effect on the TMR, while significantly reducing the junction resistance, the latter effect is believed to be caused by the prevention of FeO forming on the interface.

First-principles calculation [36] shows that an ultrathin magnesium layer inserted between iron and MgO preferentially transmits the Δ_1 band electrons, crucial for achieving large TMR. With a mono-atomic layer of magnesium, although the TMR is lower than the ideal Fe/MgO/Fe junction, it is still significantly higher than the junction with an FeO layer, which is likely to result from the deposition process of MgO without first covering the iron electrode with magnesium.

Interlayers also often produce quantum well states within them. These quantum well states can lead to oscillations in the transmission as a function of interlayer thickness and sometimes lead to negative TMR.

Reduced Symmetry Barrier Layer

Symmetry filtering is the reason for very high magnetoresistance in epitaxial tunnel junctions. All of the tunnel junctions discussed so far in this chapter have square symmetry. The MgO barrier preferentially filters Δ_1 band electrons. Another suggested cubic barrier material, $SrTiO_3$, does not provide efficient symmetry filtering. Thus, the electrode Fermi energy density of states is more important in determining the tunneling conductance through $SrTiO_3$. Consequently tunneling current through $SrTiO_3$ tends to have polarization similar to that of the Fermi energy density of states of the electrodes. In the case of Fe or Co electrodes, the minority density of states is much higher than the majority spin, so the tunneling current has a negative spin polarization. This is indeed observed experimentally.

For barrier layers that do not have cubic symmetry, can there still be efficient symmetry filtering? It turns out that for many insulators the answer may be yes.

In order to keep the epitaxial relation between the electrodes and the barrier, often the reduced symmetry of the barrier layer has to be such that its unit cell is a multiple of the square unit cell of the (100) bcc electrode. For example, consider an orthorhombic lattice with a rectangular unit cell whose side matches the bcc lattice and the *b* side is twice of the bcc lattice. Obviously the evanescent wave functions in such a barrier layer do not have cubic symmetry. The spin-filtering effect depends on how these evanescent states couple to the cubic Δ_1, Δ_2, and Δ_5 bands in CoFe and how their decay rates are relative to each other. The Δ_1 band corresponds to the reciprocal lattice vector $\mathbf{G}_0 = 0$ which is unchanged for the barrier layer. The corresponding evanescent wave in the barrier will likely have the slowest decay rate of all the complex bands. The Δ_5 band can be expressed as a linear combination of antisymmetric wave functions containing $\mathbf{G}_1$ (see section "Lateral Symmetry of Bloch States in Electrodes"),

$$|\Delta_5\rangle = A\sin[(2\pi/a)x] + B\sin[(2\pi/a)y]. \tag{134}$$

The smallest reciprocal lattice vector along the x direction is $(\pm 2\pi/a, 0)$ which is the same as the wave vector along the x direction in the electrode, and the corresponding antisymmetric evanescent state has the symmetry of $\sin[(2\pi/a)x]$. This gives us the first term in Eq. 134. The second term needs to be matched from wave functions corresponding to the reciprocal lattice vectors along the y direction. The first reciprocal lattice vector of the barrier layer is $(0, \pm 2\pi/b)$ which is half of $\mathbf{G}_1$ in CoFe. This state cannot match to the Δ_5 band in the electrode. The next reciprocal lattice vector is $(0, \pm 4\pi/b)$ which is the same as $(0, \pm 2\pi/a)$ and matches the second term in Eq. 134 perfectly. Thus, the Δ_5 state in the electrodes can be matched to a linear combination of the evanescent states corresponding to the reciprocal lattice vectors $(0, \pm 4\pi/a)$ and $(0, \pm \pi/b)$. Because of their larger transverse wave vectors, these states likely have faster decays in the direction of transmission than the evanescent wave function that matches the Δ_1 state. Therefore, if the unit cell of a reduced symmetry barrier layer is a multiple of the square unit cell of the electrode, the wave functions can be matched so that there is a likelihood that symmetry filtering will occur.

A class of materials that are being studied as barrier materials for magnetic tunnel junctions are the spinal oxides [37]. The spinels are any of a class of oxides of general formulation AB_2O_4. They usually form a cubic crystal, with the oxygen atoms arranged in a cubic close-packed lattice and the cations A and B occupying some or all of the octahedral and tetrahedral sites in the lattice. Examples of spinels that are of interest as barrier materials for magnetic tunnel junctions include $MgAl_2O_4$, $ZnAl_2O_4$, $SiMg_2O_4$, and $SiZn_2O_4$. These spinel oxides have much better lattice match with the bcc Fe or CoFe electrodes. For example, the lattice of $MgAl_2O_4$ rotated 45° produces a less than 1 % mismatch with bcc Fe along the (001) direction, compared to the more than 3 % mismatch between MgO and bcc Fe or CoFe electrodes. Due to the relatively large lattice mismatch between the bcc Fe or CoFe with MgO, the epitaxial interface usually has a large lattice strain that is likely to induce defects which in turn would reduce the TMR. Using spinel oxides as the barrier layer can greatly eliminate this problem.

The (001) crystal plane in spinel oxides has the C_{2v} symmetry. This is a different symmetry than the MgO barrier. The complex bands along the [001] direction are the $\widetilde{\Delta}_1$, $\widetilde{\Delta}_2$, $\widetilde{\Delta}_3$, and $\widetilde{\Delta}_4$ bands. These bands are listed along with the corresponding bulk bands of bcc Fe along the [001] direction in Table 3. As one can see, the complex bands in the spinels do not have a one-to-one correspondence to the Δ_1, Δ_2, $\Delta_{2'}$, and Δ_5 bands defined by the C_{4v} symmetry of the bcc electrodes. In particular, the slowest decaying complex band in the spinel oxides, $\widetilde{\Delta}_1$ band, matches to both Δ_1 and Δ_2 bands in the electrodes. However, that both Δ_1 and Δ_2 bands match to the same complex band in the spinel barrier layer does not destroy

Table 3 Fe and spinel band symmetries. The orbital composition is listed in parenthesis. The last column shows the corresponding imaginary part of the wave vector for $SiMg_2O_4$ at the Fermi energy of an $Fe/SiMg_2O_4/Fe$ junction

Fe	Rotate 45°	Spinel	$\mathrm{Im}k(2\pi/a)$
$\Delta_1(s, p_z d_{z^2})$	Δ_1	$\widetilde{\Delta}_1(sp_z d_{z^2})$	0.47
$\Delta_2(d_{x^2-y^2})$	$\Delta_{2'}$	$\widetilde{\Delta}_2(d_{xy})$	1.86
$\Delta_{2'}(d_{xy})$	Δ_2	$\widetilde{\Delta}_1(d_{x^2-y^2})$	1.84
$\Delta_5(p_x p_y d_{zx} d_{yz})$	Δ_5	$\widetilde{\Delta}_3(p_x d_{zx}), \widetilde{\Delta}_4(p_y d_{yz})$	1.04

the symmetry-filtering effect as one would naively believe. It turns out that the complex band $\widetilde{\Delta}_1$ has multiple branches. The branch that matches to the Δ_1 band has the smallest imaginary part, and the branch that matches to the Δ_2 band, even though it has the same symmetry, has a much larger imaginary part, as listed in Table 3 for $SiMg_2O_4$. Therefore, the spinel oxides can indeed serve as barrier layers that provide the symmetry filtering for spin-dependent tunneling.

Experimental measurement on single crystalline $Fe/MgAl_2O_4/Fe$ MTJs found over 110 % TMR ratio [38]. More importantly, these junctions produced large V_{half} (bias voltage at which the TMR ratio is half of that at zero bias), ranging from 1.0 to 1.3 V, significantly greater than the typical values obtained from MgO-based MTJs, which is usually about 0.5 V. The reason for the improved V_{half} is also due to the better lattice mismatch. For the MgO-based MTJs, the significant lattice strain at the interfaces produces many dislocation defects [24]. These defects can lower the magnon excitation energy which in turn lowers the TMR at finite voltages. By using a barrier layer with a better lattice match, the magnon scattering is reduced and high TMR is maintained to higher voltages.

Summary

Spin-dependent electron transport, specifically the phenomena of giant magnetoresistance and tunneling magnetoresistance, is amenable to a combination of semiclassical Boltzmann transport theory and first-principles quantum mechanical treatment. Current-in-plane giant magnetoresistance is discussed within a nonlocal semiclassical transport approximation. It is shown that CIP GMR can be treated by solving the Boltzmann transport equation for a multilayer system. The Boltzmann equation is solved using electronic structures derived from first principles for each of the layers and by taking into account the boundary conditions at the interfaces between the layers. The non-locality of the transport is less critical for current-perpendicular-to-plane GMR, but inclusion of the spin-diffusion length is critical. Spin-dependent tunneling is treated using the Landauer approach. The symmetry of the evanescent states in the insulating tunnel barrier can be used to obtain a giant TMR effect even when the tunneling electrodes are not strongly spin-polarized at the Fermi energy.

References

1. Dirac PAM (1928) The quantum theory of the electron. Proc R Soc Lond A 117:610–624
2. Grünberg P, Schreiber R, Pang Y, Brodsky MB, Sowers H (1986) Layered magnetic structures: evidence for antiferromagnetic coupling of Fe layers across Cr interlayers. Phys Rev Lett 57(19):2442–2445
3. Baibich MN, Broto JM, Fert A, Nguyen Van Dau F, Petroff F, Etienne P, Creuzet G, Friederich A, Chazelas J (1988) Giant magnetoresistance of (001)fe/(001)cr magnetic superlattices. Phys Rev Lett 61(21):2472–2475
4. Binasch G, Grünberg P, Saurenbach F, Zinn W (1989) Enhanced magnetoresistance in layered magnetic structures with antiferromagnetic interlayer exchange. Phys Rev B 39(7):4828–4830
5. Pratt WP, Lee S-F, Slaughter JM, Loloee R, Schroeder PA, Bass J (1991) Perpendicular giant magnetoresistances of Ag/Co multilayers. Phys Rev Lett 66(23):3060–3063
6. Bozorth RM (1951) Ferromagnetism. D. van Norstrand, New York, p 441
7. Chikazumi S (1964) Physics of magnetism. Wiley, New York, p 73
8. van den Berg HAM, Clemens W, Gieres G, Rupp G, Schelter W, Vieth M (1996) GMR sensor scheme with artificial antiferromagnetic subsystem. IEEE Trans Magn 32(5):4624–4626
9. Valet T, Fert A (1993) Theory of the perpendicular magnetoresistance in magnetic multilayers. Phys Rev B 48(10):7099–7113
10. Mark J, Silsbee RH (1987) Thermodynamic analysis of interfacial transport and of the thermomagnetoelectric system. Phys Rev B 35(10):4959–4972
11. Zhang X-G, Butler WH (1995) Conductivity of metallic films and multilayers. Phys Rev B 51(15):10085–10103
12. Chambers RG (1950) The conductivity of thin wires in a magnetic field. Proc R Soc A 202(1070):378–394
13. Camblong HE, Levy PM (1992) Novel results for quasiclassical linear transport in metallic multilayers. Phys Rev Lett 69(19):2835–2838
14. Fuchs K (1938) The conductivity of thin metallic films according to the electron theory of metals. Math Proc Camb Philos Soc 34(1):100–108
15. Sondheimer EH (1952) The mean free path of electrons in metals. Adv Phys 1(1):1–42
16. MacLaren JM, Zhang X-G, Butler WH, Wang X (1999) Layer KKR approach to Bloch-wave transmission and reflection: application to spin-dependent tunneling. Phys Rev B 59(8):5470–5478
17. Butler WH, Zhang X-G, Nicholson DMC, Schulthess TC, MacLaren JM (1996) Giant magnetoresistance from an electron waveguide effect in cobalt-copper multilayers. Phys Rev Lett 76(17):3216–3219
18. Butler WH, Zhang X-G, MacLaren JM (2000) Solution to the boltzmann equation for layered systems for current perpendicular to the planes. J Appl Phys 87(9):5173–5175
19. Stewart DA, Butler WH, Zhang X-G, Los VF (2003) Interfacial scattering in magnetic multilayers and spin valves. Phys Rev B 68(1):014433
20. Julliere M (1975) Tunneling between ferromagnetic films. Phys Lett A 54(1):225–226
21. Landauer R (1957) Spatial variation of currents and fields due to localized scatterers in metallic conduction. IBM J Res Dev 1(3):223–231
22. Slonczewski JC (1989) Conductance and exchange coupling of two ferromagnets separated by a tunneling barrier. Phys Rev B 39(10):6995–7002
23. Butler WH, Zhang X-G, Schulthess TC, MacLaren JM (2001) Spin-dependent tunneling conductance of Fe|MgO|Fe sandwiches. Phys Rev B 63(5):054416
24. Yuasa S, Nagahama T, Fukushima A, Suzuki Y, Ando K (2004) Giant room-temperature magnetoresistance in single-crystal Fe/MgO/Fe magnetic tunnel junctions. Nat Mater 3(12):868–871
25. Zhang X-G, Yan W, Han XF (2008) Theory of nonspecular tunneling through magnetic tunnel junctions. Phys Rev B 77(14):144431

26. Matsumoto R, Fukushima A, Nagahama T, Suzuki Y, Ando K, Yuasa S (2007) Oscillation of giant tunneling magnetoresistance with respect to tunneling barrier thickness in fully epitaxial Fe/MgO/Fe magnetic tunnel junctions. Appl Phys Lett 90(25):252506
27. Parkin SSP, Kaiser C, Panchula A, Rice PM, Hughes B, Samant M, Yang SH (2004) Giant tunnelling magnetoresistance at room temperature with MgO (100) tunnel barriers. Nat Mater 3(12):862–867
28. Yuasa S, Djayaprawira DD (2007) Giant tunnel magnetoresistance in magnetic tunnel junctions with a crystalline MgO(001) barrier. J Phys D Appl Phys 40(21):R337–R354
29. Yuasa S, Suzuki Y, Katayama T, Ando K (2005) Characterization of growth and crystallization processes in CoFeB/MgO/CoFeB magnetic tunnel junction structure by reflective high-energy electron diffraction. Appl Phys Lett 87(24):242503
30. Cha JJ, Read JC, Buhrman RA, Muller DA (2007) Spatially resolved electron energy-loss spectroscopy of electron-beam grown and sputtered CoFeB/MgO/CoFeB magnetic tunnel junctions. Appl Phys Lett 91(6):062516
31. Read JC, Cha JJ, Egelhoff WF Jr, Tseng HW, Huang PY, Li Y, Muller DA, Buhrman RA (2009) High magnetoresistance tunnel junctions with MgBO barriers and NiFeB free electrodes. Appl Phys Lett 94(11):112504
32. Yuasa S, Katayama T, Nagahama T, Fukushima A, Kubota H, Suzuki Y, Ando K (2005) Giant tunneling magnetoresistance in fully epitaxial body-centered-cubic Co/MgO/Fe magnetic tunnel junctions. Appl Phys Lett 87(24):222508
33. Yuasa S, Fukushima A, Kubota H, Suzuki Y, Ando K (2006) Giant tunneling magnetoresistance up to 410% at room temperature in fully epitaxial Co/MgO/Co magnetic tunnel junctions with bcc Co(001) electrodes. Appl Phys Lett 89(4):042505
34. Yan W, Han XF, Zhang X-G (2008) Effect of Co interlayers in Fe/MgO/Fe magnetic tunnel junctions. Appl Phys Lett 93(17):172501
35. Belashchenko KD, Velev J, Tsymbal EY (2005) Effect of interface states on spin-dependent tunneling in Fe/MgO/Fe tunnel junctions. Phys Rev B 72(14):140404
36. Wang Y, Jia Z, Zhang X-G, Hai-Ping C, Han XF (2010) First-principles study of Fe/MgO based magnetic tunnel junctions with Mg interlayers. Phys Rev B 82(5):054405
37. Jia Z, Zhang X-G, Han XF (2012) Spinel oxides: 1 spin-filter barrier for a class of magnetic tunnel junctions. Appl Phys Lett 100(22):222401
38. Sukegawa H, Xiu H, Ohkubo T, Furubayashi T, Niizeki T, Wang W, Kasai S, Mitani S, Inomata K, Hono K (2010) Tunnel magnetoresistance with improved bias voltage dependence in lattice-matched Fe/spinel $MgAl_2O_4$/Fe(001) junctions. Appl Phys Lett 96(21):212505
39. Gurney BA, Speriosu VS, Nozieres J-P, Lefakis H, Wilhoit DR, Need OU (1993) Direct measurement of spin-dependent conduction-electron mean free paths in ferromagnetic metals. Phys Rev Lett 71(24):4023–4026